BIOCHEMISTRY
including biophysical chemistry & molecular biology

Article

pubs.acs.org/biochemistry

DYNLL2 Dynein Light Chain Binds to an Extended Linear Motif of Myosin 5a Tail That Has Structural Plasticity

Andrea Bodor,[†] László Radnai,[‡,¶] Csaba Hetényi,[§] Péter Rapali,[‡] András Láng,[†] Katalin E. Kövér,[∥] András Perczel,[†,⊥] Weixiao Y. Wahlgren,[#] Gergely Katona,[#] and László Nyitray*[,‡]

[†]Laboratory of Structural Chemistry and Biology, Institute of Chemistry, and [‡]Department of Biochemistry, Eötvös Loránd University, Budapest, 1117 Hungary

[¶]Signal Transduction and Functional Genomics Research Group, Research Centre for Natural Sciences, Hungarian Academy of Sciences, Budapest, 1117 Hungary

[§]MTA-ELTE Molecular Biophysics Research Group, Eötvös Loránd University, Budapest, 1117 Hungary

[∥]Department of Inorganic and Analytical Chemistry, University of Debrecen, Debrecen, 4032 Hungary

[⊥]MTA-ELTE Protein Modelling Research Group, Eötvös Loránd University, Budapest, 1117 Hungary

[#]Department of Chemistry and Molecular Biology, University of Gothenburg, 411 37 Göteborg, Sweden

Supporting Information

ABSTRACT: LC8 dynein light chains (DYNLL) are conserved homodimeric eukaryotic hub proteins that participate in diverse cellular processes. Among the binding partners of DYNLL2, myosin 5a (myo5a) is a motor protein involved in cargo transport. Here we provide a profound characterization of the DYNLL2 binding motif of myo5a in free and DYNLL2-bound form by using nuclear magnetic resonance spectroscopy, X-ray crystallography, and molecular dynamics simulations. In the free form, the DYNLL2 binding region, located in an intrinsically disordered domain of the myo5a tail, has a nascent helical character. The motif becomes structured and folds into a β-strand upon binding to DYNLL2. Despite differences of the myo5a sequence from the consensus binding motif, one peptide is accommodated in each of the parallel DYNLL2 binding grooves, as for all other known partners. Interestingly, while the core motif shows a similar interaction pattern in the binding groove as seen in other complexes, the flanking residues make several additional contacts, thereby lengthening the binding motif. The N-terminal extension folds back and partially blocks the free edge of the β-sheet formed by the binding motif itself. The C-terminal extension contacts the dimer interface and interacts with symmetry-related residues of the second myo5a peptide. The involvement of flanking residues of the core binding site of myo5a could modify the quaternary structure of the full-length myo5a and affect its biological functions. Our results deepen the knowledge of the diverse partner recognition of DYNLL proteins and provide an example of a Janus-faced linear motif.

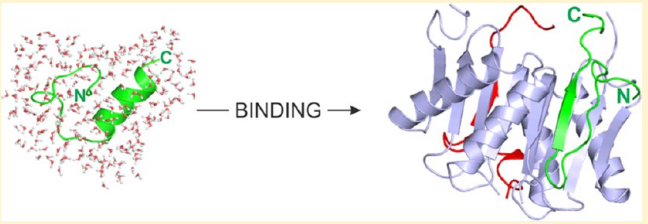

The LC8 dynein light chains were originally described as the smallest subunits of the microtubule-associated cytoplasmic dynein motor complex. They show a highly conserved amino acid sequence throughout evolution, and they were later shown to bind to more than 70 other proteins involved in various biological processes; therefore, they are now considered hub proteins.[1,2] Vertebrates contain two closely related LC8 paralogs, DYNLL1 and DYNLL2, with partially overlapping functions.[1] Under physiological conditions, LC8 proteins are stable homodimers.[3] Atomic resolution structures were determined for the apo and ligand-bound forms using X-ray crystallography and NMR spectroscopy.[4−6] Five β-strands make up two core β-sheets; one side of each sheet is flanked by two α-helices, and the other side forms the dimer interface. Strand β3 of one subunit pairs to strand β2′ of the other subunit in an antiparallel mode, and the dimer is stabilized by interface contacts through hydrophobic interactions and side chain H-bonds. Two equivalent grooves are formed, and they represent the target binding pockets of the dimer.

LC8 binding motifs are usually localized near coiled-coil or other dimerization domains in intrinsically disordered segments of their interacting proteins. Unstructured polypeptide regions are often involved in interactions that are mediated by sequential binding sites known as linear motifs.[7,8] The LC8 binding motif presents a relatively weak $[DS]_{-4}K_{-3}X_{-2}[TVI]_{-1}Q_0[TV]_1[DE]_2$ consensus sequence with a conserved glutamine in the arbitrarily chosen core position 0.[9] A few binding motifs differ considerably from the consensus sequence mentioned above; among them is myosin 5a in which position 0 is substituted with a methionine.

Received: May 14, 2014
Revised: September 8, 2014
Published: October 13, 2014

dx.doi.org/10.1021/bi500574z | *Biochemistry* 2014, 53, 7107−7122

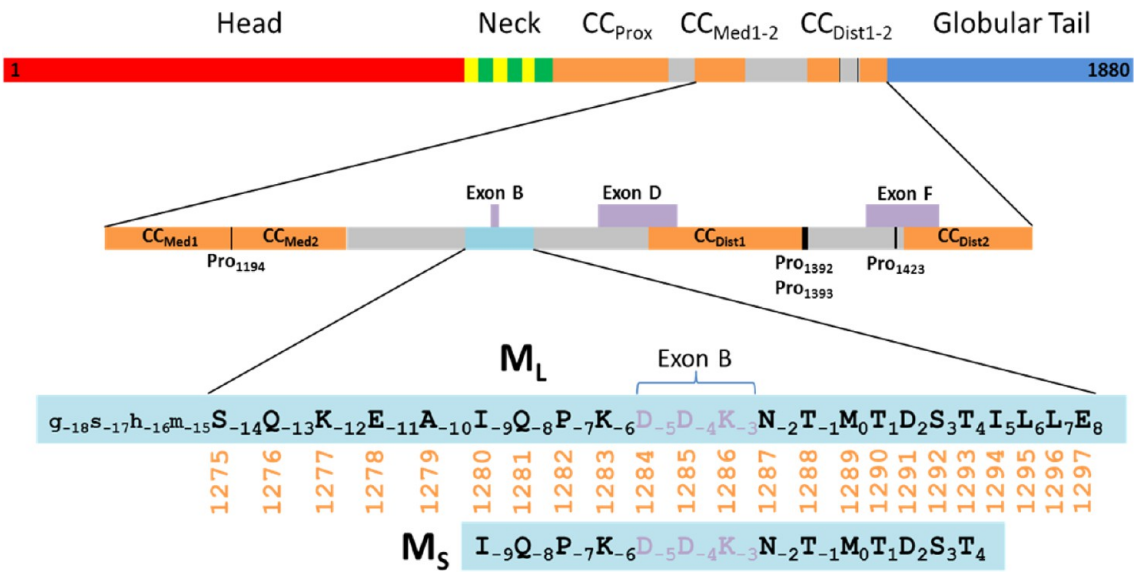

Figure 1. Bar representation of human myosin 5a (UniProt entry Q9Y4I1-3). The schematic view depicts the N-terminal motor domain (red, residues 1−765), the neck domain (residues 766−914) with six individual IQ motifs (yellow and green), and the tail domain (residues 915−1880). The latter is divided into five putative coiled-coil ("CC", orange) sequences (proximal, residues 915−1105; medial1, residues 1151−1193; medial2, residues 1195−1234; distal1, residues 1338−1391; distal2, residues 1427−1471) interrupted by non-coiled-coil regions (gray; residues 1106−1150, 1235−1338, and 1392−1426) and ends in the C-terminal globular tail domain (blue; residues 1472−1880). The region of the medial and distal CCs (enlarged) is subjected to alternative splicing. Three short exons (exons "B", "D", and "F", consisting of residues 1284−1286, 1321−1347, and 1414−1438, respectively) are expressed alternatively in different isoforms of myosin 5a; the predominant brain-specific isoform contains exon B, while the melanocyte-specific isoform contains exons D and F. Prolines interrupting the medial and distal coiled coils are also shown (black). Myosin 5a tail sequences used in this work (here termed M_L and M_S) are also depicted. The numbering of residues is according to UniProt entry Q9Y4I1-3 and is shown between M_L and M_S (orange numbers). Subscripts of the residues refer to the consensus positions of the DYNLL binding motifs. Note that four residues at the N-terminus of M_L (gshm) are cloning artifacts.

Myosin 5a (myo5a) is an intracellular motor protein involved in short-range vesicle transport along actin filaments playing various roles in different cell types.[10,11] Its structure is divided into three main parts: (i) the N-terminal motor domain responsible for force generation and ATP hydrolysis, (ii) the long, helical neck domain stabilized by the binding of six light chains, and (iii) the coiled-coil tail ending in two globular cargo binding domains[12] (Figure 1). Within the long tail domain, three coiled-coil segments, interrupted by flexible non-coiled-coil loops, are responsible for dimerization of the two heavy chains. The primary transcript of the human MYO5A gene is processed by alternative splicing.[13] Three exons within the tail domain (B, D, and F) are expressed in a cell type-specific manner; the predominant melanocyte- and brain-specific isoforms contain exons D and F and exon B, respectively.[13] The exon pattern of myo5a tail likely determines which cargo binds to the motor, because these sequences could serve as binding sites of adaptor proteins: exons D and F are necessary for the binding of Rab10 and melanophilin, respectively.[14,15] In a previous study, we identified the DYNLL2 binding motif of myo5a in a short sequence (Ile1280−Ile1294) situated between the medial and distal coiled coils of the tail.[16] The three-residue alternatively expressed exon B within the binding motif was shown to be necessary for the interaction with DYNLL2. Binding of DYNLL2 stabilizes the flanking coiled-coil sequences.[16,17] Detailed kinetic and thermodynamic characterization of this interaction using mono- and dimeric myo5a fragments revealed that the dissociation constant is somewhat weaker than that of the canonical motifs (~1−5 μM for a monomeric peptide), and bivalency of the ligand leads to pronounced avidity.[18]

LC8 proteins are subunits not only of the dynein[19] but also of the myo5a motor complex,[20] and they are known binding partners of several proteins transported by these motors (e.g., nNOS,[21,22] Pak1,[23−25] Bmf,[26] Bim,[27] Bassoon,[28] GKAP,[29] and viral proteins[30,31]). On the basis of these results, the hypothesis that DYNLL may provide a direct physical linkage between the motor and the cargos[26,28,29] was formulated. However, the majority of the binding partners (including the motors) are dimeric and, hence, bivalent ligands of LC8; highly stable dimer-to-dimer complexes are formed,[18] and the validity of the original cargo adaptor hypothesis is questioned.

Because myo5a contains a noncanonical recognition sequence that was only predicted to fit into the binding groove of DYNLL2,[16] we initiated detailed studies of this linear motif and its complex with DYNLL2 to learn the atomic details of the interaction and make suggestions about the role of the tail light chain in the transport function of the myosin motor protein. To address these goals, combined bioinformatics, NMR spectroscopy, X-ray diffraction, and molecular dynamics simulation studies were performed. NMR experiments show that the 23-residue DYNLL2 binding region of myo5a is unstructured with a nascent α-helical element in the apo form that undergoes a disorder-to-order transition and folds into a β-sheet upon formation of the complex. Our results suggest that the interacting surface in the DYNLL2−myo5a peptide complex is more extended than in other LC8−partner complexes. NMR results were supported by molecular dynamics simulations performed on the free peptide and on the complex. Working with a shorter (14 residues) myo5a peptide, we determined the crystal structure of the DYNLL2 complex at 1.85 Å resolution. The structure explains the role of the M_0 residue instead of the canonical Q_0 residue in the consensus binding sequence.

dx.doi.org/10.1021/bi500574z | *Biochemistry* 2014, 53, 7107−7122

MATERIALS AND METHODS

Cloning, Protein Expression, Peptide Synthesis, and Purification. Human DYNLL2 (UniProt entry Q96FJ2) and a fragment of human myo5a (gshmSQKEAIQPKDDKNTMTDSTILLE, UniProt entry Q9Y4I1, residues 1275−1297, hereafter termed M_L) were cloned, expressed, and purified as previously described.[16] For NMR experiments, isotope-labeled proteins were expressed in minimal medium containing $^{15}NH_4Cl$ and/or [^{13}C]glucose. The synthetic peptide (IQPKDDKNTMTDST, N-terminally acetylated, C-terminally amidated, hereafter termed M_S) corresponding to residues 1280−1293 of human myo5a was obtained from Peptide 2.0 Inc. (Chantilly, VA). The peptides were dissolved in a 0.1% TFA/water mixture and further purified by reverse-phase HPLC on a Jupiter 300 C18 (300 Å, 10 mm × 250 mm) column (Phenomenex, Torrance, CA). Elution was performed using a gradient (0 to 100%, 1%/min) of a 0.1% TFA/acetonitrile mixture. Fractions containing the peptide were pooled and lyophilized. The mass of the lyophilized powder was determined by direct measurement, and it was used later for concentration calculations. The identity and purity of the peptides were confirmed by mass spectrometry.

NMR Measurements. NMR spectra were recorded on a Bruker Avance II 500 spectrometer operating at 500.13 MHz for ^{1}H and on an Avance III 700 spectrometer operating at 700.17 MHz for ^{1}H, both equipped with 5 mm triple-resonance probe-heads with *z*-axis gradients. Sample temperatures varied in the range of 278−303 K. ^{1}H chemical shifts were referenced to the internal DSS standard, while ^{13}C and ^{15}N chemical shifts were referenced indirectly via the gyromagnetic ratios. Both ^{15}N-labeled and ^{13}C- and ^{15}N-labeled M_L samples had the following compositions: ∼0.8 mM peptide, 20 mM phosphate buffer, 20 mM NaCl, 3 mM NaN_3, 3 mM TCEP (pH 7.00), and 10% D_2O.

Sequential connectivity, backbone, and side chain resonance assignments were determined from standard triple-resonance HNCA, HN(CO)CA, HNCACB, and (H)CC(CO)NH measurements using uniformly ^{13}C- and ^{15}N-labeled peptide. ^{15}N T_1 and T_2 relaxation times and the ^{1}H−^{15}N NOE were measured using sensitivity- and gradient-improved pulse sequences. For T_1 measurements, a series of nine experiments with relaxation delay times ranging from 0.011 to 2.701 s were applied, while for T_2 measurements, relaxation delay times varied between 0.0 and 0.3 s. Errors were estimated by repetition of measurements with identical relaxation delays. The relaxation time is determined from the decay of the intensity of the corresponding ^{15}N−NH cross-peaks taken from the ^{1}H−^{15}N HSQC spectra, fitted with a two-parameter exponential decay in Sparky.[32] NOE on/off spectra were recorded in an interleaved manner with a recycle delay of 6−7 s. The {^{1}H}−^{15}N NOE is calculated as the ratio of peak intensities from the spectra acquired with and without proton saturation.

Chemical shift mapping was performed by ^{1}H−^{15}N HSQC measurements. Combined chemical shift changes were calculated for the nonoverlapping residues based on the following equation:

$$\Delta_{ppm} = [(\Delta\delta_{HN})^2 + (0.1\Delta\delta_N)^2]^{1/2}$$

where $\Delta\delta_{HN}$ and $\Delta\delta_N$ represent differences in the chemical shifts for amide protons and nitrogens, respectively, for free M_L and the DYNLL2−M_L complex, while 0.1 is the normalizing factor.[16]

^{13}C- and ^{15}N-detected saturation transfer difference (2D STD-HSQC) experiments were conducted with a sample containing 1.5 mM ^{13}C- and ^{15}N-labeled M_L and 40 μM unlabeled DYNLL2. Selective saturation was achieved by a train of 50 ms E-BURP1 (90°)-shaped pulses at −400 Hz (in the aliphatic region of the folded protein) or at 5500 Hz (the tryptophan indole peak of the protein) for a total saturation time of 2.0 s. The spectrum was recorded with 400−600 transients, and STD was monitored by either a ^{15}N HSQC or a ^{13}C CT-HSQC pulse sequence. Data were processed with TopSpin, and resonance assignment was achieved with the CARA software;[33] relaxation parameters were evaluated with Sparky.[32] Reduced spectral density mapping analysis was conducted on the basis of the work of Lefevre et al.[34,35] Spectral densities at given frequencies were calculated from the measured T_1, T_2, and heteronuclear NOE values for each amide N atom.

Protein Crystallization, X-ray Diffraction, and Model Building. DYNLL2 was dialyzed twice against TBS [20 mM Tris, 150 mM NaCl, 3 mM NaN_3, and 5 mM DTT (pH 7.6)] and concentrated using an Amicon Ultra-4 filter with an Ultracel-3 membrane (Millipore Corp., Billerica, MA). The M_S peptide was dissolved in the same buffer and subsequently complexed with DYNLL2. DYNLL2 and M_S concentrations in the final solution of the complex were 1.5 and 2.0 mM, respectively.

Crystals were grown using the hanging drop vapor diffusion method at 293 K with a reservoir solution of 1.8 M $(NH_4)_2SO_4$, 0.02 M $CoCl_2$, and 0.1 M MES (pH 6.5) and a 3.5 μL drop composed of 1 μL of reservoir solution and 2.5 μL of protein solution. Crystals appeared within 2−3 days and reached a maximum size of 0.5 mm × 0.5 mm × 0.2 mm. The crystals were soaked in reservoir solution and 20% glycerol for 1 min and subsequently flash-frozen in liquid nitrogen. Single-crystal X-ray data were collected at 100 K with an ADSC Q315R CCD detector at ID29 of the ESRF (λ = 0.93 Å). The oscillation range per image was 0.5°. Data were indexed, integrated, and scaled to a resolution of 1.85 Å using XDS and XSCALE.[36] The completeness of the data was 99.72% after the low- and high-resolution data sets had been merged. Crystals belonged to space group $P6_122$ with the following unit cell dimensions: a = b = 45.2 Å, and c = 204.0 Å. Data statistics are summarized in Table S1 of the Supporting Information.

The structure was determined by molecular replacement using PHASER[37] of the CCP4 6.1.2 Program Suite.[38] The structure of Protein Data Bank (PDB) entry 1CMI was used as a search model. After rigid body and restrained refinement with refmac5,[39] automated model building was conducted with Arp/wArp.[40] During the refinement, one cobalt(II) ion and 134 water molecules were modeled. [The cobalt(II) ion was coordinated by four nitrogen atoms and one oxygen atom of DYNLL2. These nitrogens belong to residues G_{-2}, S_{-1}, and H_0, which are cloning artifacts.] The model was then systematically improved using iterative cycles of manual rebuilding with Coot.[41] Model building was completed with an R_{cryst} of 19.3% and an R_{free} of 23.3%.

Molecular Dynamics Calculations. The M_L peptide was used for the molecular dynamics (MD) calculations. To gain information about the conformational dynamics, the peptide molecules were calculated in both unbound and protein-bound forms using the GROMACS MD software.[42] The starting

dx.doi.org/10.1021/bi500574z | Biochemistry 2014, 53, 7107−7122

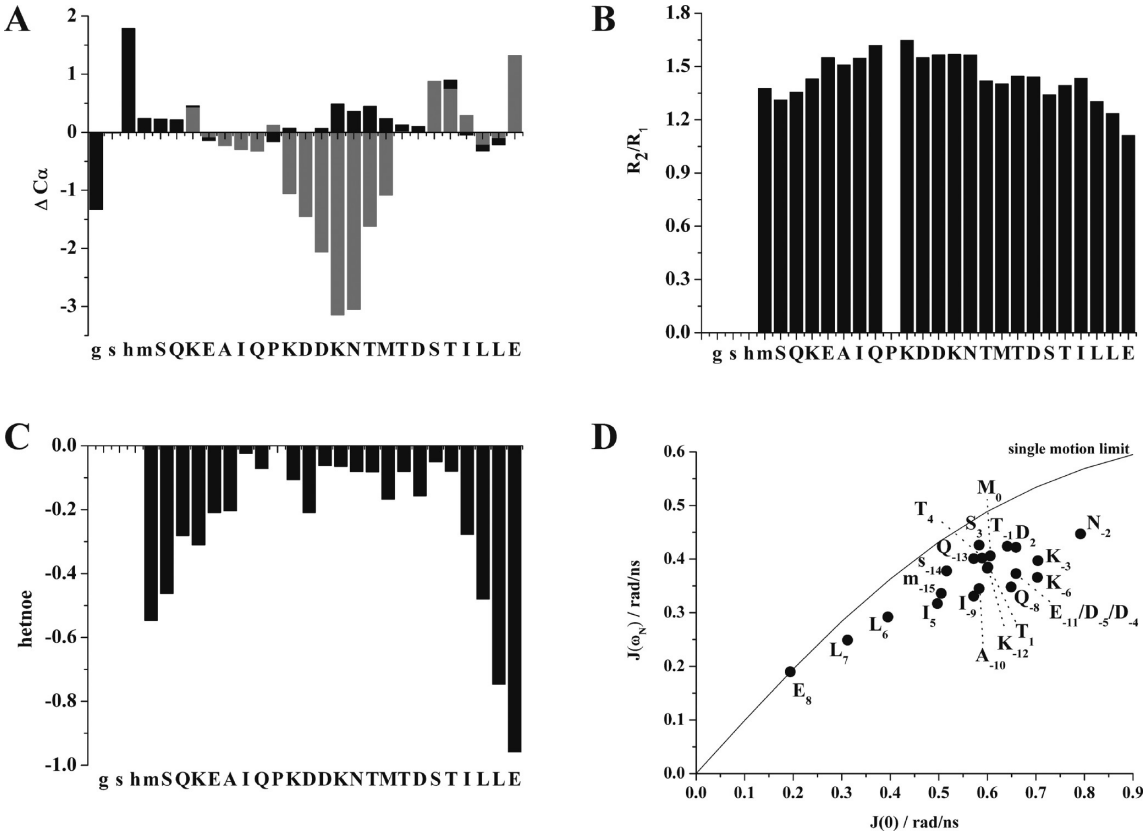

Figure 2. NMR characterization of the extended DYNLL2 binding peptide (M_L) of myo5a. (A) Secondary chemical shift values for Cα along the amino acid sequence for free (black) and DYNLL2-bound M_L (gray). (B) Variation of the R_2/R_1 ratio and (C) heteronuclear NOE enhancement along the M_L amino acid sequence. (D) Variation of $J(\omega_N)$ with $J(0)$ for M_L residues.

geometries of the DYNLL2 homodimer and the core (Q_{-8}–S_3) region of the two identical peptides and water molecules residing at the molecular surfaces were extracted from the crystallographic structure determined in this study. The missing, terminal regions of the peptide were modeled using the TINKER program package[43] and some text editing setting to the all-β-backbone conformation. In this way, the terminal parts of the bound peptide were directed toward the bulk, avoiding biased initial interactions with the protein partner. The AMBER03[44] force field was applied along with neutralizing counterions and numerous TIP3P explicit water molecules[45] filling the 9 Å space between the protein parts and the simulation box edges. The systems were refined with steepest descent and BFGS molecular mechanics energy minimizations. The refined systems were subjected to 800 ns MD simulations. A time step of 2 fs, a constant temperature of 300 K, and LINCS bond constraints were applied. Temperature coupling was conducted using the v-rescale scheme. Long-range electrostatics was calculated using the particle mesh Ewald method, and a van der Waals cutoff of 9 Å was used. Neighbor lists were updated every 10 fs. Molecular dynamics calculations were repeated for the M_L peptide (3 × 800 ns) and for the complex (M_L bound to protein, 800 ns and 2 × 320 ns) with different seed numbers used for generating the initial velocity distribution. The resulting trajectory files were analyzed with programs of the GROMACS package and the DSSP program.[46] Structural figures and movies were prepared using PyMol.[47]

Analysis of the Stability of Crystallographic Water Positions of the Protein–Peptide Interface. Structural information generated by explicit water MD calculations allowed analysis of the stability of crystallographic water positions. Setting up the stability analysis, we fit protein parts of all frames of the MD trajectory to the crystallographic protein structure to allow comparison of the surrounding water structure. The analysis was performed with a C program of C. Hetényi using the first 100 ns part of the MD trajectory. Crystallographic interface water (oxygen) positions having *B* factors of <75 Å^2 and distances of <5 Å from both the protein and peptide molecules were selected for analysis. Thus, 50 interface water positions were selected and compared to positions of 104700 water molecules of each frame of the MD trajectory. Stabilities of water positions were described calculating both the magnitudes of match and commutability of the water positions. Match is a measure of how often a calculated water molecule approaches the crystallographic water position during the MD calculations in a predefined distance threshold. The dimension of match was given in trajectory percentage, and the threshold was set to 1.5 Å. Commutability according to our definition describes how many different water molecules (distinguished by their residue numbers) stay close to the crystallographic water position in the different MD frames and for how long. The length of stay is given in trajectory percentage. Only the most frequent (the least mobile) calculated water molecules were considered for each crystallographic water positions (maximal length of stay) in this study.

RESULTS

Selection of an Extended DYNLL2 Binding Region of the myo5a Heavy Chain. We analyzed the sequence of

dx.doi.org/10.1021/bi500574z | *Biochemistry* 2014, 53, 7107–7122

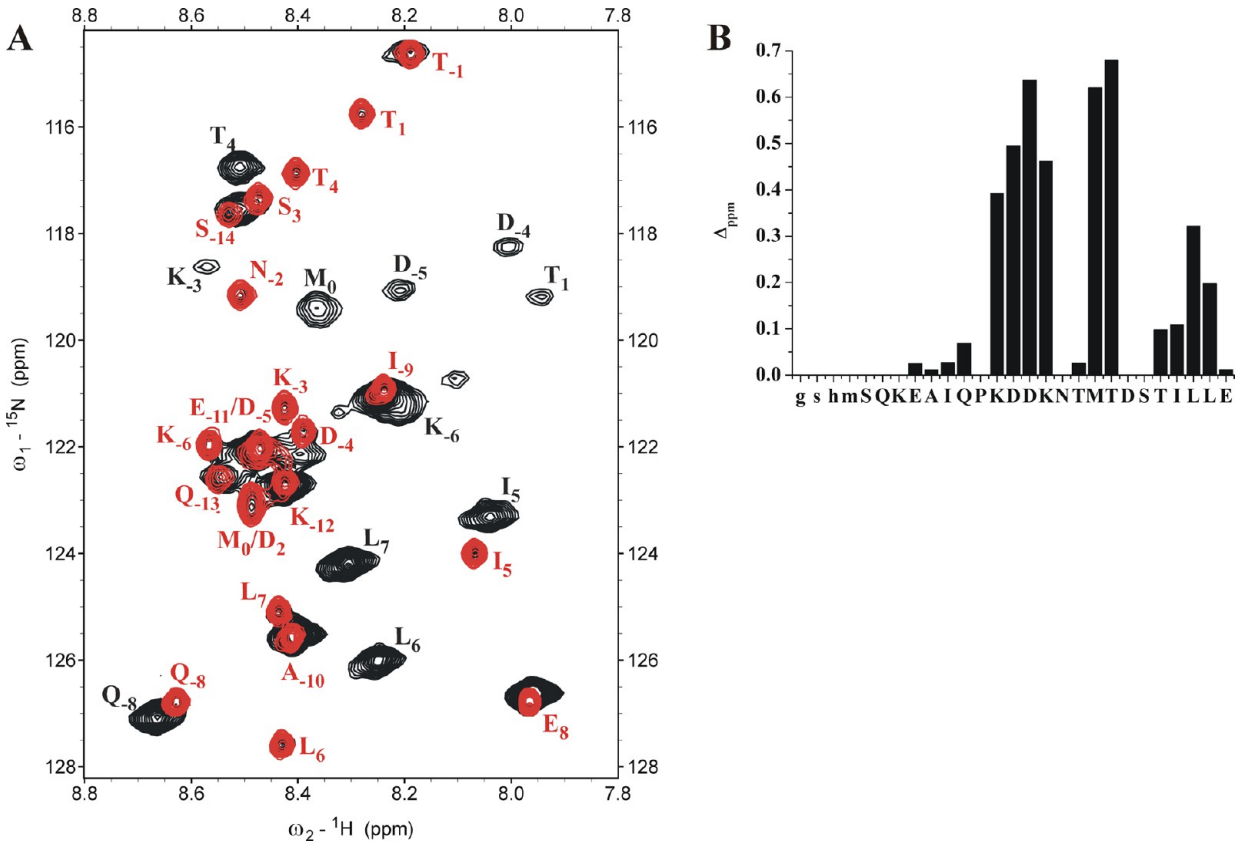

Figure 3. Chemical shift mapping of complex formation of the M_L peptide with DYNLL2. (A) Overlap of the 700 MHz ^{1}H−^{15}N HSQC spectra for free (black) and DYNLL2-bound (red) M_L at 288 K. (B) Combined chemical shift changes (parts per million) along the sequence. Missing values are due to spectral overlap or peaks broadened below the baseline.

myo5a by coiled-coil (COILS),[48] disorder (IUPred),[49,50] and disordered binding motif (ANCHOR)[51,52] predicting algorithms. The tail region (V915−V1855) begins just after the last IQ motif of the neck. As expected, COILS predicted three main coiled-coil regions in the tail: the proximal (V915−V1105), the medial (D1151−A1234), and the distal (V1338−G1446 in isoform 1 containing exons B and D, I1313−G1419 in isoform 2 corresponding to the predominant brain-specific splice form, and I1313−G1471 in isoform 3 corresponding to the predominant melanocyte-specific splice form) coiled coils.

The medial coiled coil is disrupted by a proline residue [P1194 (Figure 1)]. Similarly, two adjacent prolines disrupt the distal coiled coil (P1392 and P1393 in isoforms 1 and 3 and P1365 and P1366 in isoform 2). Interestingly, these disruptions are almost exactly in the center of their respective coiled-coil regions (before and after the breaks there are ∼40 and ∼50 residues in the case of the medial and distal coiled coils, respectively). Moreover, coding sequences of the alternatively spliced exons D (in isoforms 1 and 3) and F (in isoform 3) cause only negligible changes in the length of these coiled-coil segments: exon D extends the C-terminal part of the non-coiled-coil region between the medial and distal coiled coils, while exon F introduces a new proline (P1423 in isoform 3) into the sequence, giving rise to the chance of the formation of a new, ∼30-residue non-coiled-coil region flanked by the two segments of the distal coiled coil.

Exon B encodes only three residues (DDK, 1284−1286) within the non-coiled-coil segment between medial and distal coiled coils. IUPred predicted both long and short disorder around this region. Interestingly, while ANCHOR predicts binding sites within exons D and F, there is no binding site predicted within this disordered region. Taking into account the result of these predictions, we have chosen the long disordered region between S1275 and E1297 as an extended DYNLL2 binding motif (Figure 1) for further NMR experimental analysis (M_L peptide, numbered here as S_{-14}−E_8).

NMR Characterization of the Extended DYNLL2 Binding Motif of myo5a. *Resonance Assignment.* The 27-residue M_L consists of mainly hydrophilic residues with a small hydrophobic inner part ($A_{-10}I_{-9}$) and a hydrophobic C-terminus ($I_5L_6L_7$). Note that the four N-terminal residues are from the expression vector. Confirming the IUPred analysis no tendency for structural ordering is observed. Both ^{1}H and ^{1}H−^{15}N HSQC spectra have low signal dispersion, and most NMR resonances fall close to the average random-coil value, resulting in signal overlap for several residues, as seen in Figure 3A. ^{15}N-edited NOESY spectra showed only sequential connectivity, which is clear evidence of a lack of secondary structural elements under the given experimental conditions. Secondary chemical shifts (SCSs) were calculated using temperature- and sequence-corrected random-coil chemical shift values.[53,54] SCS data for $\Delta C\alpha$ (Figure 2A), $\Delta(C\alpha\text{-}C\beta)$, and $\Delta H\alpha$ (Table S2 of the Supporting Information) along the amino acid sequence have values around zero, an indicator of disordered structure. On the other hand, in the D_{-4}−T_4 segment, an inherent helical preference is observed: $\Delta H\alpha$ values are slightly negative, and the corresponding $\Delta C\alpha$ and $\Delta C\alpha$-$C\beta$ values are slightly positive. Compared to the values obtained for a real helix, the helical tendency of this region is around 10% at 288 K. This observation is valid for the M_L

dx.doi.org/10.1021/bi500574z | *Biochemistry* 2014, 53, 7107−7122

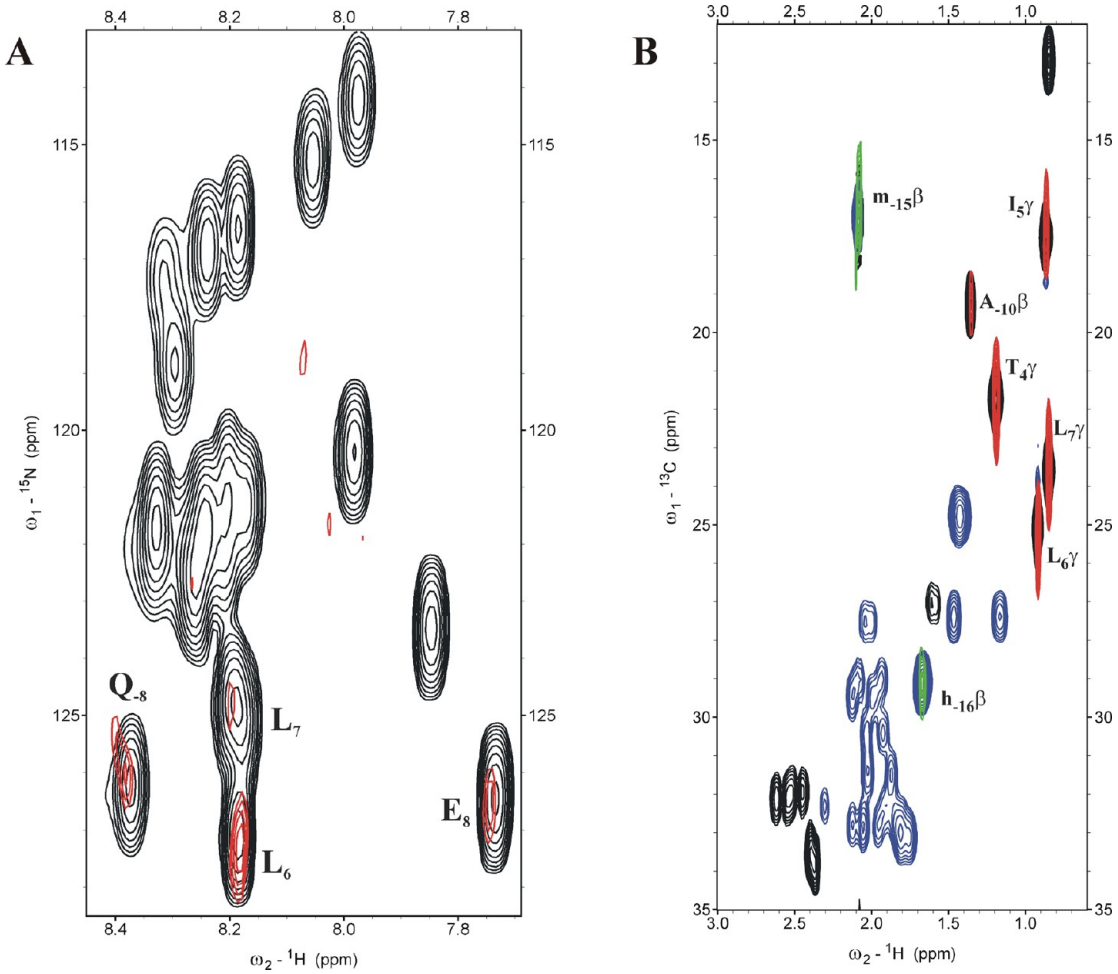

Figure 4. STD-HSQC measurements. (A) Overlap of the 500 MHz $^{1}H-^{15}N$ HSQC (black) and STD-HSQC (red) spectra at 290 K (protein irradiation at 5500 Hz). (B) Overlap of the 500 MHz $^{1}H-^{13}C$ CT-HSQC (black for CH and CH_3, blue for CH_2) and STD-(CT)-HSQC (green for CH and CH_3, red for CH_2) spectra at 290 K (protein irradiation at −400 Hz).

segment and cannot be safely extended to the intact protein. However, an increase in temperature causes higher mobility, and therefore, under physiological conditions, the fragment will be mostly in the unfolded state.

Relaxation Parameters and Reduced Spectral Density Mapping Analysis. ^{15}N relaxation rates (R_1 and R_2) of the free M_L show an unsymmetrical bell-like profile with a plateau decreasing toward the C-terminus. The N-terminus is highly mobile because the corresponding peaks are below the detection limit. The R_2/R_1 ratio along the sequence falls in the region of 1.0−1.4 (Figure 2B), indicating that the ^{15}N relaxation is mostly dominated by higher-frequency motions. Heteronuclear NOE values are more negative toward both N- and C-termini, showing a variation between −0.90 and −0.03, in accordance with fast motions and high flexibility. Greater NOE enhancements are obtained for the $D_{-4}-T_{-1}$ region, and the highest value is found at I_{-9} indicating that slower motions characterize these residues (Figure 2C).

Our results suggest that the relaxation of the $I_{-9}-T_{-1}$ region is not influenced or is the least influenced by the segmental motions of the backbone atoms (picosecond to nanosecond scale). On the basis of these relaxation parameters (Table S3 of the Supporting Information), the reduced spectral density mapping analysis allows a more direct evaluation of the relative degree of motion at ω_N, $0.87\omega_H$, and zero frequencies ($\omega_0 = \nu_0 2\pi$). Restricted motions toward the microsecond time scale are indicated by larger $J(0)$ values, as observed for the $K_{-6}-N_{-2}$ region with a local maximum at N_{-2}, while all other residues fall in the vicinity of the single motion limit curve (Figure 2D), indicating higher backbone flexibility. The overall conclusion to be drawn from the NMR relaxation data is that free M_L is rather flexible and has a quite unstructured backbone; however, a weak but noticeable helical tendency is detected in the central region accommodating the core recognition motif of $D_{-4}-T_1$. We cannot directly extend this conclusion to the full-length myosin 5a heavy chain; however, these results suggest that the connecting region between the medial and distal coiled-coil domain is mostly unstructured with some propensity to fold into an α-helix around $D_{-4}-T_1$.

Formation of the Complex of the Extended myo5a Peptide with DYNLL2. *Chemical Shift Mapping.* Successive addition of unlabeled DYNLL2 to the ^{13}C- and ^{15}N-labeled myo5a fragment results in the formation of a 2:2 complex (consisting of 232 residues in total). A molecule of such size tumbles slower in solution than the M_L partner does, and as a consequence, it will present broader peaks in the spectra. Figure 3A shows the overlay of $^{1}H-^{15}N$ HSQC spectra obtained at 288 K for the free and DYNLL2-bound M_L. As formation of this complex is slow on the NMR time scale, two sets of peaks appear; the narrow and broad sets belong to the free and

dx.doi.org/10.1021/bi500574z | *Biochemistry* 2014, 53, 7107−7122

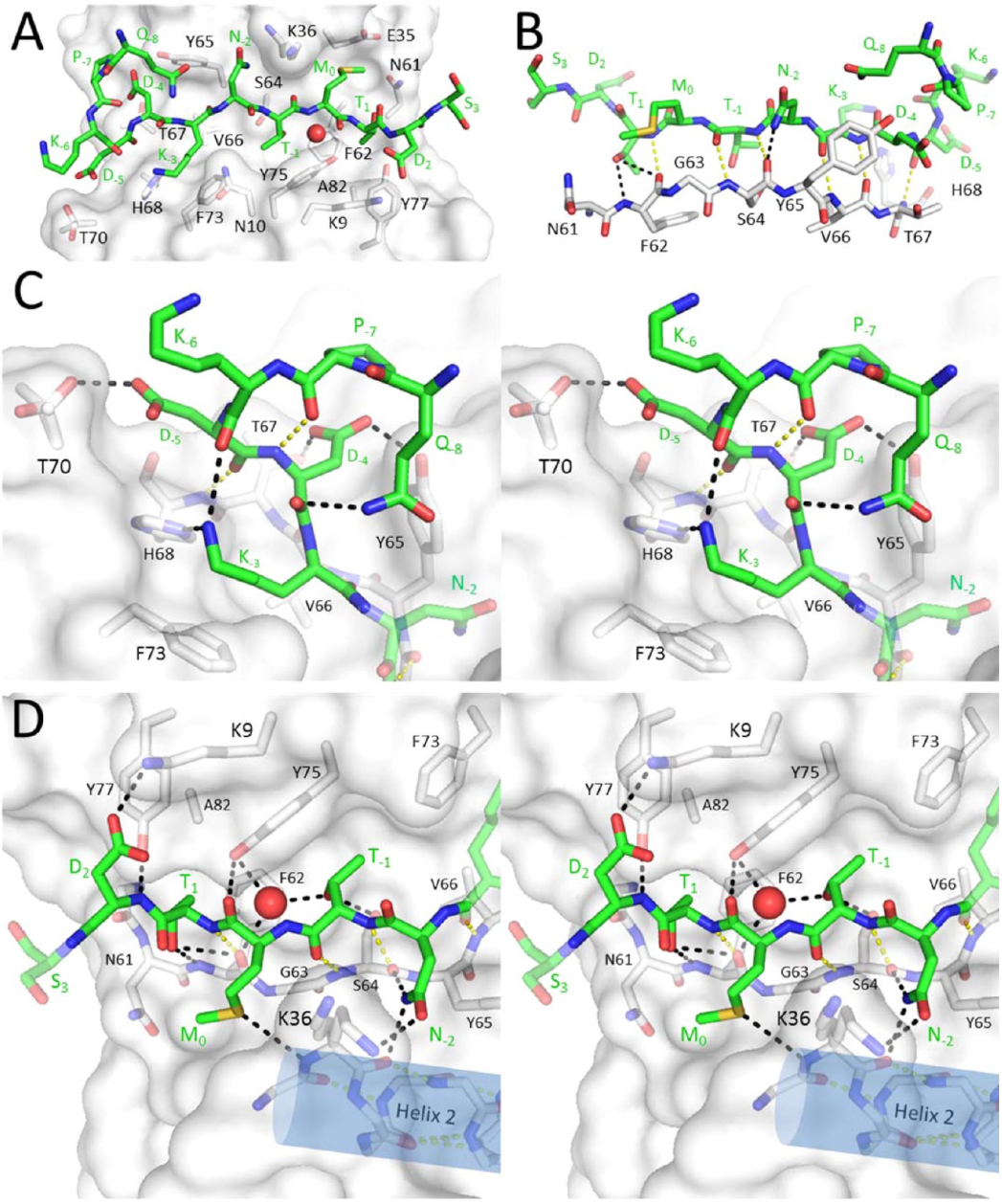

Figure 5. Structure of the DYNLL2−M_S complex at 1.8 Å resolution. (A) Binding groove with the M_S peptide (DYNLL2, gray; myo5a, green). (B) β-Sheet formation (main chain H-bonds, yellow; side chain H-bonds, black). (C) Interactions of Q_{-8}−K_{-3}. K_{-3}, D_{-4}, and D_{-5} (corresponding to exon B) are involved in multiple interactions with DYNLL2. Three residues (K_{-6}, P_{-7}, and Q_{-8}) turn back toward the binding groove and make multiple interactions with residues K_{-3}−D_{-5}. These interactions block the potential hydrogen bond donor and acceptor groups of the peptide backbone around position −4 (cross-eye stereoview). (D) Interactions of N_{-2}−D_2. Helix capping by M_0. One water molecule (directly beneath M_0, shown here as a red sphere) forming hydrogen bonds simultaneously with the peptide and DYNLL2 can be found in the majority of other known crystal structures (cross-eye stereoview).

complexed M_L, respectively. The intensity of the free M_L peaks decreases, while the intensity of those of the complex increases. Several peaks undergo very large chemical shift variations; therefore, assignments for the DYNLL2−M_L complex peaks had to be obtained separately from triple-resonance measurements. Regions K_{-6}−K_{-3} and M_0-T_1 show the largest shifts (Figure 3B). ^1H−^{13}C CT HSQC measurements (Figure S1 of the Supporting Information) reveal the disappearance of Cα, Cβ, and Cγ atoms in the Q_{-8}−T_1 region; decreasing intensities are observed for the I_{-9} environment and the D_2−L_7 region, while intensities of the G_{-18}−A_{-10} and E_8 residues remain unchanged. On the other hand, calculated SCS values for Cα (Figure 2A) and Cα-Cβ (Table S4 of the Supporting Information) are highly negative for the K_{-6}−T_1 region, indicating formation of a β-sheet upon complexation. We conclude that the K_{-6}−T_1 region is the primary binding site. In parallel, the intrinsic helicity characteristic of the free peptide transforms into a pronounced secondary structural element, adopting a β-sheet structure when binding to DYNLL2.

Saturation Transfer Difference (STD) Measurements. A ligand-detected STD experiment is one of the most powerful methods for determining binding sites on the ligand, with the best performance for K_d values in the micromolar to millimolar range.[55] Note that the K_d of M_L with DYNLL2 was measured

dx.doi.org/10.1021/bi500574z | *Biochemistry* 2014, 53, 7107−7122

to be ≈9 μM.[18] As DYNLL2 is a well-folded protein, the region of choice for selective irradiation corresponds to the strongly shifted methyl resonances situated between −1 and −2 ppm. While the M_L fragment has no tryptophan residue, DYNLL2 possesses one, thus allowing selective saturation around the indole environment at 10 ppm. Performing both the conventional ^{1}H STD and the group-selective STD experiments, we obtained weak STD signals. However, because of severe signal overlap in the obtained 1D STD spectra, no unequivocal assignment could be assessed for the bound residues. Using ^{13}C- and ^{15}N-labeled M_L, the initial ^{1}H STD experiment could be appended with two-dimensional (2D) ^{15}N HSQC or 2D ^{13}C CT-HSQC sequences. As shown in Figure 4A, STD effects were detected for the Q_{-8}, L_6, and E_8 residues and to a lesser extent for the L_7 backbone NH. The ^{13}C STD-(CT)-HSQC spectrum proved to be more informative (Figure 4B), highlighting several affected methyl groups: the overlapping Cγ2s for I_{-9} and I_5, the overlapping Cδ1 and Cδ2 for L_6 and L_7, the overlapping Cγ2s for T_{-1}, T_1, and T_4, Cβ resonances for A_{-10}, Cε for M_{-15}, Cβ environments of H_{-16} (M_{-15} and H_{-16} are derived from the expression vector) and K_{-6}, Cγs for E_{-11} and E_8, and Cα for L_6 and L_7. Thus, STD results highlight the M_L−DYNLL2 interaction in a residue-specific manner. In particular, the hydrophobic contacts were revealed covering the T_4−E_8 and E_{-11}−I_{-9} segments, and some additional residues (T_1, T_{-1}, and K_{-6}). The binding seems tighter at the C-terminus of M_L, and the role of the side chains in complex formation will be discussed below.

Crystal Structure of DYNLL in Complex with the Binding Motif of Myosin 5a. The inherent flexibility of the N- and C-terminal ends of the M_L hindered crystallization of the DYNLL2−M_L complex. However, removal of several residues from both termini resulted in the shorter M_S peptide (Figure 1) that proved to be suitable for crystallization, and the structure of the DYNLL2−M_S complex could be determined at 1.85 Å resolution.

The overall conformation of DYNLL2 in the complex strongly resembles those found in other complex structures of this family (PDB entries 1CMI,[5] 3DVP,[56] 3E2B, 2P2T,[57] 2PG1,[58] 3FM7, 3GLW,[59] 3P8M, and 2XQQ[9]). One M_S peptide is bound to each binding groove of DYNLL2 (Figure 5A). The walls of the grooves are defined mainly by side chains of aromatic residues (F62, Y65, H68, F73, Y75, and Y77). At the bottom of the grooves, six hydrogen bonds [M_S D_{-5}(CO) to DYNLL H68(NH), M_S K_{-3}(NH) to V66(CO), M_S K_{-3}(CO) to V66(NH), M_S T_{-1}(NH) to S64(CO), M_S T_{-1}(CO) to S64(NH), and M_S T_1(NH) to F62(CO))] connect the backbone atoms of M_S with the edge of the outer β-strands of DYNLL2, thereby extending the β-sandwich core by a new antiparallel β-strand (Figure 5B). The core binding motif begins with three residues corresponding to exon B ($D_{-5}D_{-4}K_{-3}$). The side chains of these residues make extensive contacts with DYNLL2: the carboxyl group of D_{-5} forms a hydrogen bond with the hydroxyl group of T70, the carboxyl group of D_{-4} forms hydrogen bonds simultaneously with the hydroxyl groups of T67 and Y65, and the methylene groups of K_{-3} have hydrophobic contacts with the aromatic ring of F73, while the amino group at the end of this side chain forms a hydrogen bond with N^{ε} of H68 (Figure 5C).

We have previously shown that the myo5a splice variant lacking exon B does not bind to DYNLL2.[16] If D_{-5}, D_{-4}, and K_{-3} were missing from M_S, they would be replaced in the complex by Q_{-8}, P_{-7}, and K_{-6}, respectively. As the exchange of K_{-3} with another Lys would not cause any difference, the other two positions must be responsible for the dramatic affinity reduction. As stated above, D_{-5} forms one hydrogen bond with T70. Gln has a side chain somewhat longer and more flexible than that of Asp. Because both D_{-5} and T70 are located at the surface of the complex, it seems to be very likely that Gln could also make a similar hydrogen bond at this position without making significant strains in the structure due to the longer side chain. However, the replacement of D_{-4} with a Pro would make it impossible to form two hydrogen bonds (with the hydroxyl groups of T67 and Y65) and probably would force the N-terminal end of the peptide (Q_{-8} in this case) to form a conformation in which the backbone hydrogen bond at the preceding position (between Q_{-8} and H68) could not form either. The loss of these hydrogen bonds and the possible shortening of the β-strand explain why exon B is necessary for binding of myo5a to DYNLL2.

In addition to the three residues corresponding to exon B, five more (N_{-2}, T_{-1}, M_0, T_1, and D_2) residues of M_S make direct contacts with DYNLL2 (Figure 5). The side chain of N_{-2} is within hydrogen bonding distance of two backbone carbonyl groups of DYNLL (K36 and S64) and the amino group at the side chain of K36. As expected,[16] the central TQT motif of the canonical sequences is replaced with the $T_{-1}M_0T_1$ motif at an equivalent position. The hydroxyl group of the side chain of T_{-1} plays a special role in the complex, forming a hydrogen bond both with the hydroxyl group of S64 and with a water molecule deeply wedged between the peptide and DYNLL2. This water molecule is also within hydrogen bonding distance of a hydroxyl group (Y75) and a carbonyl oxygen (F62) of DYNLL2 (Figure 5D).

The noncanonical M_0 residue adopts a conformation very similar to the conformation of the typical Q_0, and it is able to participate in similar interactions at the surface of DYNLL2 (see Discussion). The antiparallel β-strand conformation of the peptide ends at T_1, because there is a hydrogen bond between the backbone nitrogen atom of F62 and the hydroxyl group of the side chain of T_1, instead of the carbonyl oxygen of T_1 (Figure 5B,D). At this point, the peptide turns outward from the binding groove. Interestingly, neither M_0(CO) nor D_2(NH) is involved in β-sheet formation, but M_0(CO) and D_2(NH) make hydrogen bonds with the hydroxyl groups of Y75 and Y77, respectively. These hydrogen bonds help to hold the planes of the respective peptide bonds in a "rotated" position, resulting in the side chain of T_1 turning toward the bottom of the binding groove to break the hydrogen bonding network of the antiparallel β-strand, and leading the peptide out from the binding groove. This conformation is further stabilized by a salt bridge between D_2 and K9 (Figure 5D).

The most remarkable feature of the complex is the N-terminus of M_S (Q_{-8}, P_{-7}, and K_{-6}). Although the quality of the electron density map was poor in this region, this short stretch of residues could be identified in the structure in an unexpected position. The peptide backbone makes a β-turn-like structure (hydrogen bond between the carbonyl oxygen of P_{-7} and the NH group of D_{-4}), and the N-terminus of M_S folds back toward the core binding motif, making several favorable interactions with residues corresponding to exon B. The most important interactions stabilizing this conformation are two additional hydrogen bonds, one between the carbonyl oxygen of K_{-6} and the NH group of K_{-3} and another between the carbonyl oxygen of D_{-4} and the side chain amide nitrogen of Q_{-8} (Figure 5D). Although the weak electron density and high

dx.doi.org/10.1021/bi500574z | Biochemistry 2014, 53, 7107−7122

B factors of the atomic model indicate that the positions of these residues are not well-defined, this conformation is unique among DYNLL−partner complexes and may also have some biological significance. Atomic details of this "backfolding" of the myo5a heavy chain peptide were further investigated by MD simulations.

Molecular Dynamics Simulation of the myo5a Peptide in Free Form and in Complex with DYNLL2. To complement the results obtained by NMR spectroscopy and X-ray crystallography, we conducted MD simulations both with free M_L and with the DYNLL2−M_L complex. These simulations provided more information about the behavior of the DYNLL binding motif, especially about the N- and C-terminal extensions, because the quality of the electron density map was poor at the N-terminus of the M_S in the crystal complex, and any attempts to crystallize DYNLL2 with M_L were unsuccessful. MD is also the method best suited to the study of the role of water molecules mediating the interaction between myo5a and DYNLL2. Three repeated MD runs were performed for both the unbound M_L peptide and its complex with DYNLL2 to assess the statistical reliability of the results (Figure S4 of the Supporting Information). The overall secondary structure shows low variability between MD runs in the core region of M_L.

During MD runs, the unbound M_L quickly lost its bound (partially β-sheet) geometry observed in the crystal structure and used as an initial structure for the calculation, and a bend → turn → α-helix conformational transition of the D_{-4}−M_0 sequence was observed (Figure 6 and Figures S4 and S5 Movie S1 of the Supporting Information). Remarkably, the stabilization of the α-helical structure for the D_{-4}−T_1 core region is in accordance with our NMR spectroscopic analysis, namely, that this region has a propensity to fold into an α-helix.

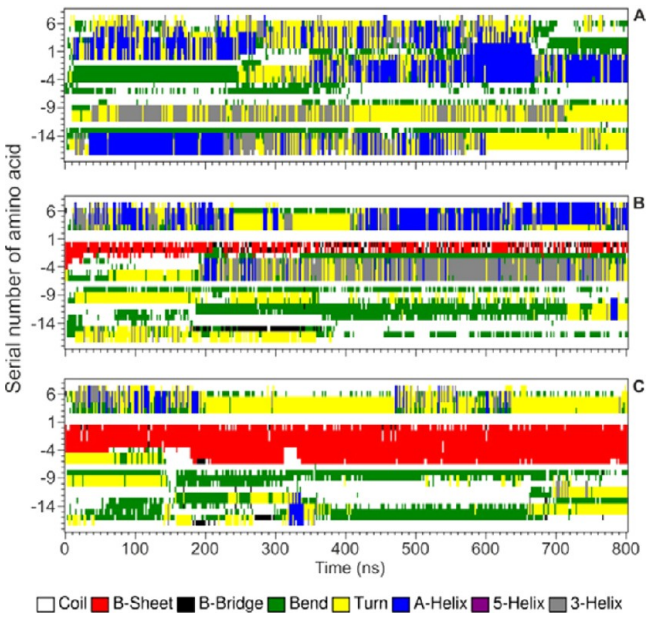

Figure 6. Time evolution of the secondary structure of the M_L peptide in the free state (A) and bound to DYNLL2 (B and C). The partially β-sheet (DYNLL2-bound) backbone conformation of the M_S crystal structure was used as a starting (t = 0 ns) geometry for all molecular dynamics calculations. The β-sheet quickly disappeared in free solution (A) and is practically not visible in this plot. In the DYNLL2-bound forms, the β-sheet remained stable for short (B, chain B) and large (C, chain D) sections of M_L.

As mentioned above, the K_{-3}−M_0 region of the peptide is in an antiparallel β-sheet arrangement in the crystal structure of the DYNLL2−M_S complex. Repeated MD calculation of the complex also confirms this finding and emphasizes that the stabilization center of the β-sheet is at the T_{-1} and M_0 core residues, where both copies (chains B and D) of the peptide remained in the β-sheet in all three MD runs (Figure 6 and Figures S4 and S5 and Movie S2 of the Supporting Information). In the case of chain D, this region extends to the K_{-3}−M_0 region, whereas for chain B, the appearance of the nativelike unbound secondary structure is located at the central T_{-1} and M_0 residues and also observed with high variability at K_{-3} and N_{-2}. However, this reduction of the antiparallel β-region does not lead to dissociation of the peptide. The N- and C-terminal parts of the bound peptide do not remain in the extended all-β conformation set as the initial conformation (see Materials and Methods). Both termini quickly bend over the neighboring parts of the protein (Movie S2 of the Supporting Information) and occasionally adopt helical and β-turn conformations at the N-terminal extension and make hydrophobic contacts with symmetry-related residues of the second myo5a peptide at the C-terminal extension during the MD simulations (Figure 6 and Figure S3 and Movie S1 of the Supporting Information).

Stability of Crystallographic Water Positions at the Protein−Peptide Interface. Fifty crystallographic water molecules residing in the protein−peptide interface were selected for molecular dynamics-based stability analysis. Among them, seven water positions were identified as being remarkably stable, i.e., having a calculated positional match of larger than 10%, and the least mobile calculated water with a maximal length of stay of >10% at the same time (Table S5 of the Supporting Information). Two of the seven water molecules showed extreme stability with 75 and 96% matches and 100−100% lengths of stays, respectively (Figure S6 of the Supporting Information). This water molecule deeply wedged between the peptide and DYNLL2 (Figure 5B). Stable crystallographic water positions and the most stable positions with the best overall score of 100% are highlighted in Table S5 of the Supporting Information with blue and red spheres, respectively. Notably, stable positions are located mainly at the C-terminal end of the β-strand part of the bound DYNLL2 peptide.

DISCUSSION

The Unstructured DYNLL2 Binding Motif of Myosin 5a Shows a Weak Helical Tendency and Folds into a β-Sheet upon Interacting with DYNLL2. In solution, the free M_L shows a very dynamic and highly unstructured nature with a tendency to adopt helices (~10% helicity detected) as proven both by NMR spectroscopy and by MD simulations. Measured relaxation rates are in the average range for the whole molecule, showing local minima in the hydrophobic core at residue I_{-9} for both R_2 and R_1. It is known that R_1 average relaxation rates for disordered proteins do not vary dramatically if they are measured at the same field strength. For the 27-residue M_L peptide, this value (R_1^{av}) is 3.03 ± 0.54 s^{-1} at 280 K. It was expected that the K_{-6}−D_2 region, including the exon B-encoded residues and the core motif, should be responsible for binding to DYNLL2. In free M_L, heteronuclear NOE values show the most positive values in the I_{-9}−T_4 region in

dx.doi.org/10.1021/bi500574z | *Biochemistry* 2014, 53, 7107−7122

accordance with the increased structural propensity that coincides perfectly with the indicated inherent helical tendency of the K_{-6}–T_4 region indicated by Hα SCS data. The spectral density function at zero frequency reveals regions with restricted motions on the subnanosecond time scale for residues that bear a larger than average $J(0)$ value. In this respect, the K_{-6}–K_{-3} segment fulfills this criterion, and again, it is in full agreement with the inherent helicity of this region. However, we should add that at near physiological temperatures the nascent helical tendency of M_L is diminishing. IDPs and IDP segments have the tendency to show mostly inherent helical regions,[60−62] and the corresponding segments often bear important functional characteristics or contain the binding motifs to partner proteins. A consequence of interaction with the binding partner is the folding of the unstructured region, and formation of all major secondary structure types (helix, sheet, and coil) is possible. There are proteins, like the disordered C-terminal domain of the p53 hub protein, that (depending on the binding partner) can fold into all three secondary structure types.[63] Currently, the functional relevance of the helical tendency of the DYNLL binding linear motif is not known. It is possible that the nascent helix is more stable in the case of the full-length protein by forming a local helix bundle or is stabilized by interacting with a so far unknown binding partner. Ubiquitination of nearby residues may also change the stability of the nascent helix (see below).

The disorder-to-order transition of the M_L upon binding to DYNLL2 results in the formation of a β-sheet. Proof is obtained from calculated SCS data for both Cα and (Cα-Cβ) resonances: the pronounced negative SCS values in the K_{-6}–M_0 region indicate the presence of a β-sheet. On the other hand, chemical shift mapping results show that the K_{-6}–T_1 segment is the main binding site. All our results emphasize that working with a relatively short peptide accommodating the binding sequence allows us to gather information about the resulting secondary structure of the folded and/or complexed state (this one being the first example for the LC8 protein family).

Benison et al. conducted an NMR study of formation of the complex between the N-terminal domain of the dynein intermediate chain (IC84−143) and *Drosophila* LC8.[64,65] The IC84−143 segment contains the highly conserved "TQT box", and binding to LC8 caused broadening below the detection limit of the peaks belonging to the residues involved in binding; a similar broadening effect was observed for M_L, while the peaks of the residues outside the binding sequence remained unperturbed and maintained the disorder state outside the binding region. On the other hand, here we show not only the partial folding of the unbound M_L but also the structural transition into a β-sheet upon interaction with DYNLL2, an example of structural plasticity in a short linear motif (Figure 7). Previously, we have shown by kinetic studies that the binding of DYNLL isoforms to their various partners can be best described by a conformational selection model.[18] The region of the free myo5a peptide contains an inherent α-helix that should be in the unfolded state to fit into the binding groove of DYNLL2; this finding is consistent with a conformational selection mechanism for the formation of DYNLL complexes.

The Noncanonical Recognition Motif of myo5a Binds to the Binding Groove of DYNLL2 Like Other Known Binding Partners. All partners (including the noncanonical myo5a and Pak1) bind to DYNLL by extending one of the β-

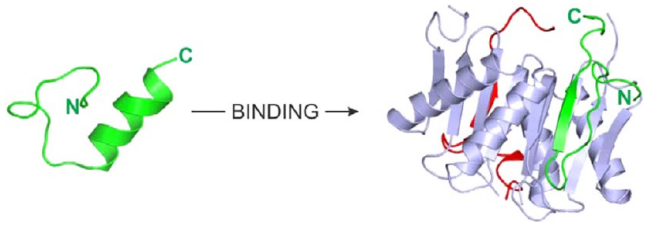

Figure 7. Conformational transition of the M_L peptide between the free and DYNLL-bound form. A large structural transition of M_L (green) could be observed upon formation of the complex with DYNLL2 (gray) by MD simulation. The transient α-helix of unbound M_L disappeared, and a β-strand was developed in both chain B (green) and chain D (red) copies of the peptide. The N-terminal end of the peptide was found to be in a bend/turn region with a high degree of curvature (see also Figure 6 for a detailed per-residue analysis of the secondary structures of both chains). In the case of chain B, the N-terminal end of the peptide bent over the C-terminal region. Only one M_L chain is shown in the free form. The C-terminal ends of the peptides in the complex tend to interact via hydrophobic residues.

sheets in the β-sandwich core of DYNLL by a new, antiparallel strand. Side chains of adjacent residues in an antiparallel β-strand point in alternating directions (Figure 8A). This arrangement minimizes the possible side chain to side chain contacts in the motif and maximizes the independence of the individual positions. The surface of DYNLL provides different binding pockets for each position. Close examination of the binding groove reveals that side chains at positions 1, 0, −1, and −3 accommodate the best defined, deep pockets of DYNLL. Residues in other positions are directed toward the solvent and/or are accommodated in a more permissive, shallow pocket and, thereby, have less interaction with DYNLL. These observations are in good agreement with the results of phage display experiments[9] as well as with *in silico* analysis of the contribution of key residues and their context with respect to the global binding energy.[66]

The backbone of bound polypeptides in all structures occupies almost the same position within the groove of DYNLL (Figure 8B). This mainly results from the antiparallel β-sheet conformation. The hydrogen bonding network necessary for antiparallel β-sheet formation usually starts at position −6 and ends at position 1 (Figure 8B). The DYNLL1−nNOS complex (PDB entry 1CMI) is an exception in which the β-sheet extends to the NH group at position 3 (Figure 8C). All DYNLL recognition motifs, except in nNOS and Pak1, have a Thr at position 1 (T_1). As we have already discussed, the hydroxyl group of T_1 of myo5a makes a hydrogen bond with the backbone NH group of F62. For this interaction, the side chain of T_1 must turn downward toward the bottom of the groove. The Val in nNOS (V_1) in the same position is unable to form hydrogen bonds with the backbone of DYNLL1; that is why the side chain of V_1 turns outward and forces Y75 and Y77 of DYNLL1 into a distorted position (Figure 8C), thus preventing the interaction. These changes caused by V_1 propagated an effect along the backbone of DYNLL, forcing the entire binding groove to adopt a more open conformation.[4] The width of the binding groove (defined as the distance between C63 and C9 α-carbon atoms of DYNLL[4]) is 12.3, 13.4, and 14.2 Å, in the case of free DYNLL, the LC8−Swallow complex (another "T_1"-type ligand), and the DYNLL1−nNOS complex, respectively.[4] This distance is 13.2 Å in the case of DYNLL2−myo5a and DYNLL2−EML3 complexes,[9] and indeed, both the peptide backbones and the T_1

dx.doi.org/10.1021/bi500574z | *Biochemistry* 2014, 53, 7107−7122

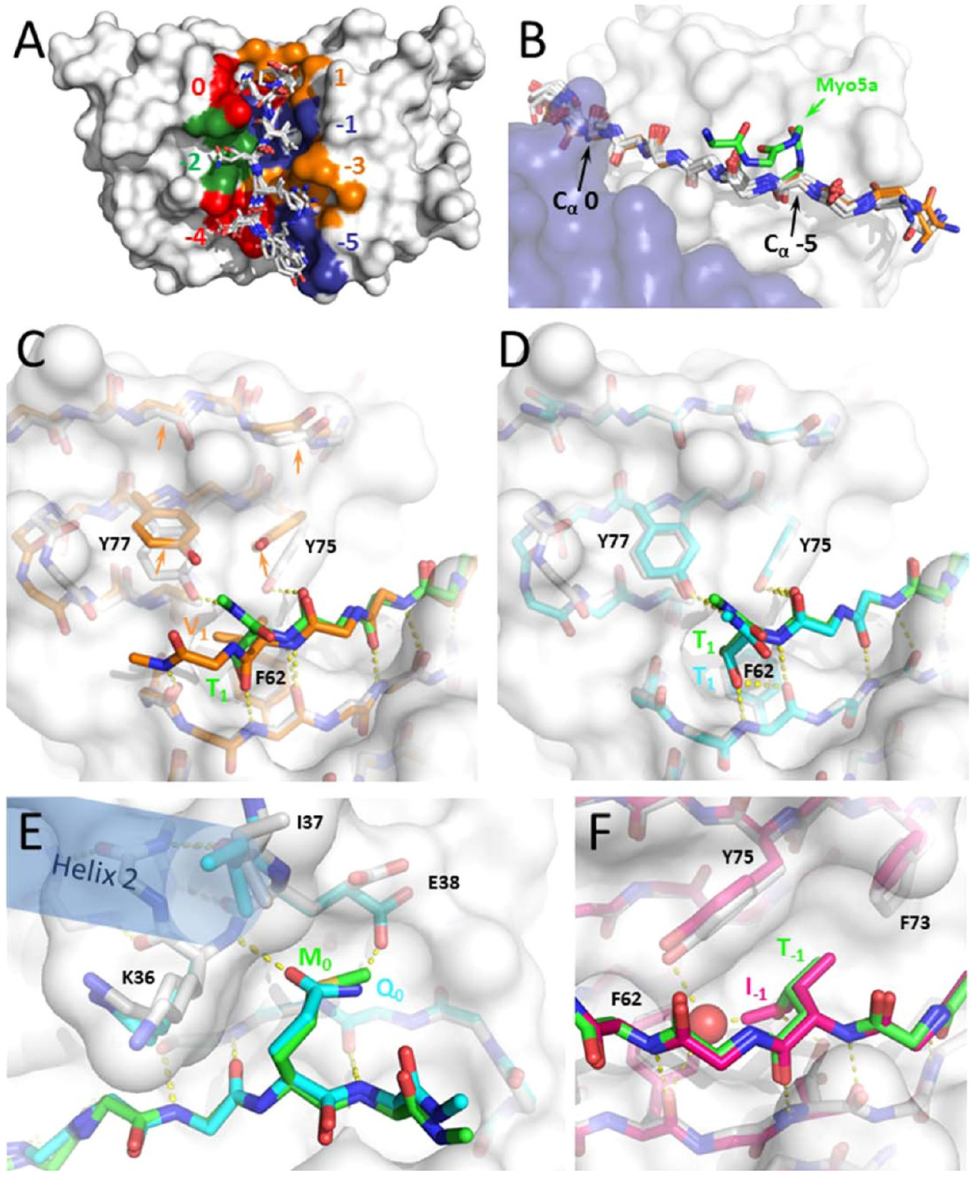

Figure 8. Structural comparison of the DYNLL2−M_S complex with other known DNYLL−peptide complexes. (A) Individual binding pockets of DYNLL (positions are numbered according to the arbitrary numbering of residues within bound motifs). All known crystal structures (PDB entries 3P8M, 2XQQ, 2P2T, 3ZKE, 1CMI, 4DS1, 4HT6, 3DVP, and 3E2B) were superimposed. Binding motifs are represented as sticks. For the sake of simplicity, only the surface of the DYNLL2−M_S complex is shown. (B) Backbones of the bound peptide motifs within the groove of DYNLL show very similar conformations. The surface of the two subunits of DYNLL2 is colored blue and white. Note that uniquely among the binding motifs the backbone conformation of M_S (green) at position −5 folds back on itself. (C) Binding pocket 1 for M_S (T_1, green) and for nNOS (V_1, orange, PDB entry 1CMI). The side chain of T_1 turns downward and forms a hydrogen bond with the backbone of DYNLL2. The side chain of V_1 in nNOS protrudes bellow the rings of Y77 and Y75 and thereby forces the whole binding groove to open more widely (indicated by orange arrows). (D) Binding pocket 1 for M_S (T_1, green) and for EML3 (T_1, cyan) (PDB entry 2XQQ). Conformations of both the peptide ligands and DYNLL2 are highly similar. (E) The Met (M_0) in M_S (green) and the conserved Gln (Q_0) in EML3 (cyan) adopt similar conformations in the binding pocket of position 0. Gln is involved in capping of helix 2 (at the backbone NH group of K36) and also forms a hydrogen bond with the side chain of E38 (white and cyan in the DYNLL2−M_S and DYNLL2−EML3 complexes, respectively). The sulfur atom of Met can form only a weak interaction with the backbone NH group of K36. The hydrogen bond to the side chain of E38 is missing in this case. (F) Binding pocket −1 for M_S (T_{-1}, green) with a water-mediated interaction and for NUP159 (I_{-1}, magenta) (PDB entry 4DS1). Ile is too bulky to allow the incorporation of a water.

side chains of these ligands superimpose very well as shown in Figure 8D.

Position 0 is the most conserved among the binding motifs. Except myo5a and Pak1, all partners have a Gln in this position. The side chain of Q_0 caps one of the α-helices of DYNLL by making a hydrogen bond with the backbone NH group of K36 (Figure 8E). Both side chain and main chain atoms of K36, E35, and I34 participate in the formation of the well-defined pocket accommodating Q_0. The volume of the pocket would allow only residues that are equal in size or smaller than a Gln in this position. The chemical features of the pocket clearly explain why Glu and Asp, holding a net negative charge, are not allowed in this position (would cause an electrostatic repulsion). On the other hand, small and medium sized, uncharged, polar (e.g., Asn) or hydrophobic (e.g., Leu) residues are not preferred in this position either because of the loss of

dx.doi.org/10.1021/bi500574z | *Biochemistry* 2014, 53, 7107−7122

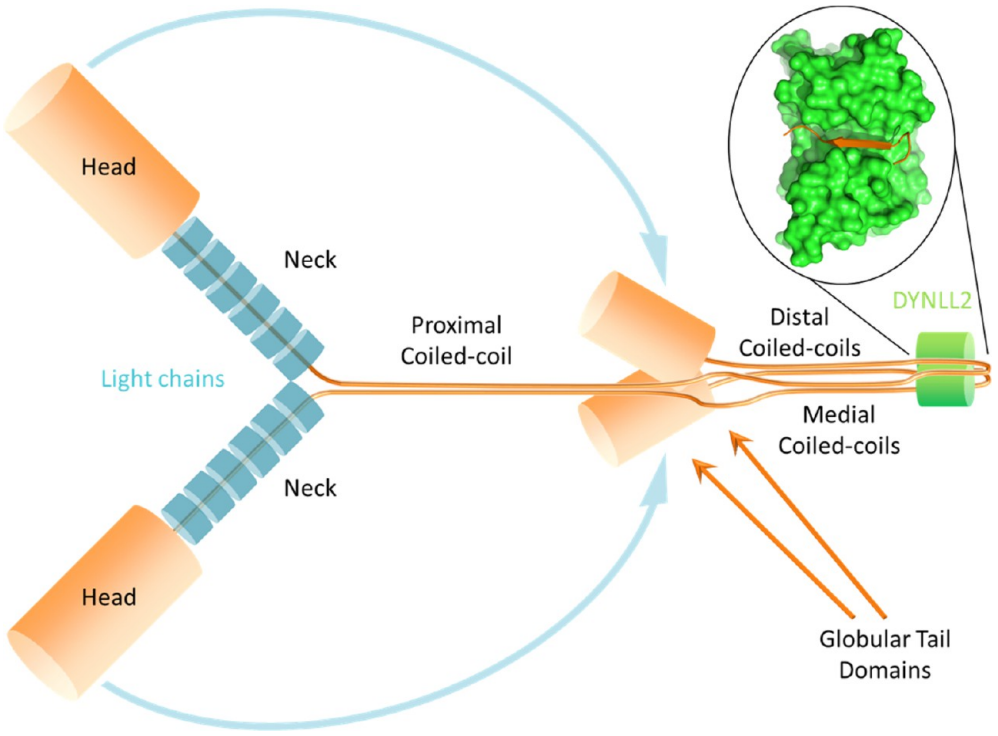

Figure 9. Hypothetical model of the asymmetric folding of myosin 5a. The structure of the DYNLL2−M_L complex determined in this work is shown above the medial and distal coiled coils of the tail region (DYNLL2, surface, green; M_L, cartoon, orange). Blue arrows represent the movement of the motor domains required for the formation of the off state, where the heads directly interact with the GTDs.

two important intermolecular hydrogen bonds. Such a loss of stability is somewhat compensated by S_0 in Pak1 by forming a side chain H-bond with the amino group of K36. However, M_0 in myo5a fits almost perfectly into the binding pocket, and its side chain accommodates the same position as does Q_0 in other partners (Figure 8E). Although the sulfur atom can form a weak H-bond with the backbone NH group of K36, this residue is clearly suboptimal at this position of the groove. Weaker binding is evidenced by smaller K_d values: for TQT motifs (e.g., in Bmf), the affinity is 1 μM, while for the TMT motif in myo5a, the affinity is 9 μM.[18] This weaker affinity apparently does not interfere with the function of the tail light chain, for the bivalency and therefore avidity of the binding motif[18] result in the formation of a stable complex between the two proteins despite the noncanonical Met at position 0. This conclusion is confirmed by our extended phage display experiments in which the conserved Gln was allowed to mutate to any residue and Met-containing, besides Gln-containing, dimeric peptides were selected as strong binders to DYNLL1.[a]

Thr and Ile are the most common residues in position −1 of the motifs.[9] They are all accommodated in the deepest pocket formed by Y75, F73, F62, L84, and S64 residues of the binding groove (Figure 8F). Interestingly, all crystal structures with bound peptides having a Thr in this position reveal the same interaction pattern, including the deeply wedged water molecule and the hydrogen bond network connecting DYNLL and T_{-1} via this water (Figure 5D). This is in good agreement with our conclusions based on the crystal structure of the DYNLL2−M_S complex and with the results of MD simulations presented here. The contacts of the T_{-1} side chain were detected also by STD NMR experiments. Binding of the bulkier side chain of I_{-1} in other structures seems to restrict any water molecule to remain in this pocket, most probably by simply limiting the space available for the water. Loss of the hydrogen bond network provided by this water is probably compensated by the favorable entropic effect related to the burial of more hydrophobic surfaces. This is in good agreement with our previous results showing that the entropic contribution is the largest in the case of the nNOS peptide compared to those of other partners.[18]

Position −2 shows no obvious amino acid preference. However, *in vitro* evolution showed some preference for the bulky, aromatic side chain of Trp in this position.[9] On the basis of our structural comparison, the binding pocket seems to be shallow and relatively permissive here. Side chains in this position face mostly toward the solvent and make only a few contacts with DYNLL. myo5a seems to be a special case according to the importance of position −2. As shown above, the side chain of N_{-2} is within hydrogen bonding distance of the backbone carbonyl groups of residues K36 and S64 of DYNLL. Moreover, the carbonyl oxygen of N_{-2} makes a hydrogen bond with the amino group of K36 (Figure 5D). As M_0 of myo5a is a suboptimal residue, one would expect a compensatory mechanism with a positive contribution to the binding strength at another site. The observed interactions of N_{-2} may represent this expected mechanism.

DYNLL2 Binding and Folding of the Myosin 5a Tail. Cargo binding of myo5a has been shown to be regulated by proteolysis, phosphorylation, and Ca^{2+} binding.[67] At low levels of Ca^{2+} and in the absence of cargos, the motor adopts a closed, triangle-like conformation. In the inactive conformation, the heads fold back and directly interact with the globular tail domains (GTDs).[67] However, if all the coiled-coil domains and the inter-coiled-coil regions were in an extended conformation, the length of the neck domains would not allow the heads to reach the GTDs. Indeed, the GTDs were shown to interact

dx.doi.org/10.1021/bi500574z | *Biochemistry* 2014, 53, 7107−7122

with the C-terminal part of the proximal coiled-coil region, and this interaction was proven to be necessary for the binding of the heads in the inactive conformation.[68] It is obvious that the direction of the myosin 5a heavy chains must be totally reversed in this conformation to allow the GTDs to reach the proximal coiled coil. The tail reversal most likely occurs in a non-coiled-coil region harboring the binding motif of DYNLL2 flanked by the medial and distal coiled coils. Theoretically, the GTDs can fold back in a symmetric or asymmetric fashion. Detailed analysis of pictures obtained by electron microscopy indicates that the rotational symmetry of the dimeric myosin molecule is not preserved in the inactive conformation.[69] This strongly supports the second model. If we suppose that the medial and distal coiled coils remain intact and are roughly equal in length, then the inter-coiled-coil region with the DYNLL2 binding site seems to be the only probable "breakpoint" in the inactive conformation in the myo5a tail (Figure 9). The resulting asymmetry must influence the conformation of the whole myo5a molecule (at least in the inactive state), because each GTD is oriented differently relative to the proximal coiled coil.

In this work, we have shown by X-ray crystallography, NMR spectroscopy, and MD simulations that the unstructured fragment of the myo5a tail corresponding to the DYNLL2 binding site and flanking sequences tends to fold upon the binding of the tail light chain. As revealed by our crystal structure, the N-terminal extension ($Q_{-8}P_{-7}K_{-6}$) tends to fold back and interact with the free β-edge of the bound sequence itself. STD NMR measurements and MD simulations also showed this tendency. These findings are in good agreement with our theoretical considerations: not only the position relative to the medial and distal coiled coils but also the inherent malleability of the unstructured DYNLL2 binding site makes this sequence the most probable site of chain reversal in the myo5a tail (Figure 9), and binding of DYNLL2 might be important in stabilizing the reversed conformation. Nevertheless, one should keep in mind that the tail light chain could be involved in the regulation only of the myosin 5a isoforms that contain the exon B-encoded sequence, e.g., in the neuronal-specific isoform. To the best of our knowledge, there was only one report addressing the role of the tail light chain in the regulation of myo5a.[70] The authors concluded that binding of DYNLL2 is apparently not required for adopting the inhibitory folded conformation of the motor protein. However, we noted that a full-length myo5a heavy chain clone lacking exon B was used in those experiments; therefore, the recombinant protein could not bind the tail light chain. In light of our results, reexamining the role of DYNLL2 in the regulation of this myosin motor would be worthwhile.

The function of the C-terminal extension (D_2–E_8) seems to be much simpler. Our STD measurements and MD simulations showed that this sequence not only interacts with the side of the canonical binding groove (side of the dimer interface) but also weakly dimerizes. Hydrophobic contacts and backbone hydrogen bonds in the $I_5L_6L_7$ region play a key role in the dimerization tendency (Movie S1 of the Supporting Information). These results suggest that DYNLL2 can promote the stabilization of the N-terminal part of the distal coiled coil by holding the heavy chains of the full-length myosin in the proximity (especially in isoforms where exon D is not present). Such a "molecular glue" stabilization function of DYNLL has been previously shown in the case of myo5a[16,17] and other binding partners.[71,72]

Interestingly, the myo5a heavy chain has two known ubiquitination sites within the N-terminal extension of the DNYLL binding region (K_{-6} and K_{-12}) (found in the PhosphoSite database[73]). Ubiquitination is an important post-translational modification regulating degradation, cellular localization, and interactions of many proteins.[74] The unstructured and flexible DYNLL2 binding site may be easily accessible for ubiquitin ligases. On one hand, binding of DYNLL2 promotes the folding of this region, and the resulting stability (decreased flexibility) may affect the activity of ubiquitin ligases on residues K_{-6} and K_{-12}. On the other hand, ubiquitination may also influence DYNLL binding and/or the conformation of this region. Consequently, both DYNLL binding and ubiquitination could have important roles in the regulation of myo5a.

DYNLL as a Cargo Binding Adaptor. Could DYNLL binding be involved in (or interfere with) the cargo transport function? Previously, we have proposed a potentially novel cargo binding mechanism[1] based on the crystal structure of DYNLL2 in complex with a recombinant, dimeric protein fragment corresponding to the DYNLL binding motif of EML3, a microtubule binding protein involved in mitosis.[9] As in the case of other known partners, the linear binding motifs of EML3 lie in the binding grooves and extend the structural core of DYNLL dimers by forming new β-strands. However, the new edges of the β-sheets protrude toward the environment, giving them a chance to form other β-sheet-mediated interactions. So far, such interactions have been reported only as crystal contacts between the DYNLL complexes within the crystal structure mentioned above.[9]

Free β-edges are common indicators of protein–protein interaction sites.[76,77] In the crystal structure presented in this work, the N-terminal part of the myo5a peptide folds back and blocks some positions on the exposed β-edge (NH and CO of the residue in position −4) by forming hydrogen bonds. Interestingly, the same positions are involved in the peculiar crystal contacts of the EML3 complex. These together indicate a potential binding site on the surface of all DYNLL complexes and provide some support for the new cargo binding hypothesis. Moreover, if a cargo (DYNLL–cargo complex) competes with the N-terminal extension of the DYNLL binding motif, the latter must be displaced from the original "reversed" position. The effects of this displacement can influence the conformation of the whole tail region and the GTDs and, most importantly, the interaction between the GTDs and heads. Further investigations of the possible "heteromer β–β" interactions and refinement of the structure of the coiled-coil tail are necessary to test the validity of this hypothesis.

CONCLUSION

In this work, we found that the DYNLL recognition motif of the myosin 5a motor protein, despite deviations from the consensus motif ("TMT" instead of "TQT"), accommodates the same binding groove of this eukaryotic hub protein as do all its other partners. Moreover, the binding motif is extended toward both termini compared to the core consensus sequence. The binding motif of the "tail light chain" (DYNLL2) of myosin 5a is embedded in an intrinsically disordered segment of the tail, between the medial and distal coiled-coil domains. Interestingly, the DYNLL recognition segment has a nascent helical tendency in the free form and undergoes an α-helix to β-chain transition (apparently via a random-coil state) upon complex formation; i.e., it is a sequence within the myosin 5a tail that shows high malleability, a general feature of linear

dx.doi.org/10.1021/bi500574z | Biochemistry 2014, 53, 7107–7122

motifs and molecular recognition elements in IDPs.[75] Finally, we suggest that the bound DYNLL could be involved in the stabilization of the folded off state of myosin 5a isoforms (e.g., in brain cells) that contain the exon B-encoded sequence.

■ ASSOCIATED CONTENT

Supporting Information

Results of the equivalence of the binding positions in the two DYNLL2 grooves as studied by NMR spectroscopy (Figure S2), analysis of the stability of crystallographic water positions at the protein−peptide ligand interface (Figure S6 and Table S5), crystallographic data statistics (Table S1), $^{1}H-^{13}C$ CT HSQC measurements of the DYNLL2−M_L complex (Figure S1), measured NMR chemical shift values and calculated secondary chemical shifts at three different temperatures (Tables S2 and S4), and relaxation parameters (Table S3). This material is available free of charge via the Internet at http://pubs.acs.org.

Accession Codes

Atomic coordinates of the DYNLL2−M_S complex have been deposited in the Protein Data Bank as entry 4D07.

■ AUTHOR INFORMATION

Corresponding Author

*Phone: 36-13812171. Fax: 36-13812172. E-mail: nyitray@elte.hu.

Author Contributions

A.B. and L.R. contributed equally to this work.

Funding

The work was supported by the Hungarian National Research Fund (OTKA Grants NK81950 and K108437 to L.N., NK101072 to A.P., and K105459 to K.E.K.), the Swedish Research Council (Grants 2011-6516 and 2009-350 to G.K.), and a János Bolyai Research Scholarship from the Hungarian Academy of Sciences (to A.B.). The European Union and the European Social Fund have provided financial support to the project under Grant Agreement TÁMOP 4.2.1./B-09/KMR-2010-0003.

Notes

The authors declare no competing financial interest.

■ ACKNOWLEDGMENTS

We thank the beamline staff at ID29 of the European Synchrotron Radiation Facility for their expert assistance during data collection and the National Information Infrastructure Development Institute of Hungary for computational infrastructure and time provided by the NIIF supercomputing facility. We acknowledge PRACE for awarding us access to resources at Monte Rosa based in Switzerland at the CSCS Swiss National Supercomputing Centre and NIIFI SC based in Hungary at the NIIF National Information Infrastructure Development Institute.

■ ABBREVIATIONS

CT-HSQC, constant time heteronuclear single-quantum coherence; DSS, 4,4-dimethyl-4-silapentane-1-sulfonic acid; DYNLL1 and -2, LC8 vertebrate LC8 dynein light chain isoforms; HSQC, heteronuclear single-quantum coherence; IDP, intrinsically disordered protein; myo5, myosin 5a; MES, 2-(*N*-morpholino)ethanesulfonic acid; NMR, nuclear magnetic resonance; NOE, nuclear Overhauser effect; R_1, longitudinal relaxation rate constant; R_2, transverse relaxation rate constant; SCS, secondary chemical shift; STD, saturation transfer difference; T_1, longitudinal relaxation time; T_2, transverse relaxation time.

■ ADDITIONAL NOTE

[a]P. Rapali, L. Radnai, G. Pál, and L. Nyitray, unpublished results.

■ REFERENCES

(1) Rapali, P., Szenes, A., Radnai, L., Bakos, A., Pal, G., and Nyitray, L. (2011) DYNLL/LC8: A light chain subunit of the dynein motor complex and beyond. *FEBS J. 278*, 2980−2996.

(2) Barbar, E. (2008) Dynein light chain LC8 is a dimerization hub essential in diverse protein networks. *Biochemistry 47*, 503−508.

(3) Barbar, E., Kleinman, B., Imhoff, D., Li, M., Hays, T. S., and Hare, M. (2001) Dimerization and folding of LC8, a highly conserved light chain of cytoplasmic dynein. *Biochemistry 40*, 1596−1605.

(4) Benison, G., Karplus, P. A., and Barbar, E. (2008) The interplay of ligand binding and quaternary structure in the diverse interactions of dynein light chain LC8. *J. Mol. Biol. 384*, 954−966.

(5) Liang, J., Jaffrey, S. R., Guo, W., Snyder, S. H., and Clardy, J. (1999) Structure of the PIN/LC8 dimer with a bound peptide. *Nat. Struct. Biol. 6*, 735−740.

(6) Fan, J., Zhang, Q., Tochio, H., Li, M., and Zhang, M. (2001) Structural basis of diverse sequence-dependent target recognition by the 8 kDa dynein light chain. *J. Mol. Biol. 306*, 97−108.

(7) Dunker, A. K., Silman, I., Uversky, V. N., and Sussman, J. L. (2008) Function and structure of inherently disordered proteins. *Curr. Opin. Struct. Biol. 18*, 756−764.

(8) Neduva, V., Linding, R., Su-Angrand, I., Stark, A., de Masi, F., Gibson, T. J., Lewis, J., Serrano, L., and Russell, R. B. (2005) Systematic discovery of new recognition peptides mediating protein interaction networks. *PLoS Biol. 3*, e405.

(9) Rapali, P., Radnai, L., Suveges, D., Harmat, V., Tolgyesi, F., Wahlgren, W. Y., Katona, G., Nyitray, L., and Pal, G. (2011) Directed evolution reveals the binding motif preference of the LC8/DYNLL hub protein and predicts large numbers of novel binders in the human proteome. *PLoS One 6*, e18818.

(10) Hammer, J. A., III, and Sellers, J. R. (2012) Walking to work: Roles for class V myosins as cargo transporters. *Nat. Rev. Mol. Cell Biol. 13*, 13−26.

(11) Langford, G. M. (2002) Myosin-V, a versatile motor for short-range vesicle transport. *Traffic 3*, 859−865.

(12) Trybus, K. M. (2008) Myosin V from head to tail. *Cell. Mol. Life Sci. 65*, 1378−1389.

(13) Lambert, J., Naeyaert, J. M., Callens, T., De Paepe, A., and Messiaen, L. (1998) Human myosin V gene produces different transcripts in a cell type-specific manner. *Biochem. Biophys. Res. Commun. 252*, 329−333.

(14) Roland, J. T., Lapierre, L. A., and Goldenring, J. R. (2009) Alternative splicing in class V myosins determines association with Rab10. *J. Biol. Chem. 284*, 1213−1223.

(15) Wu, X., Wang, F., Rao, K., Sellers, J. R., and Hammer, J. A., III (2002) Rab27a is an essential component of melanosome receptor for myosin Va. *Mol. Biol. Cell 13*, 1735−1749.

(16) Hodi, Z., Nemeth, A. L., Radnai, L., Hetenyi, C., Schlett, K., Bodor, A., Perczel, A., and Nyitray, L. (2006) Alternatively spliced exon B of myosin Va is essential for binding the tail-associated light chain shared by dynein. *Biochemistry 45*, 12582−12595.

(17) Wagner, W., Fodor, E., Ginsburg, A., and Hammer, J. A., III (2006) The binding of DYNLL2 to myosin Va requires alternatively spliced exon B and stabilizes a portion of the myosin's coiled-coil domain. *Biochemistry 45*, 11564−11577.

(18) Radnai, L., Rapali, P., Hodi, Z., Suveges, D., Molnar, T., Kiss, B., Becsi, B., Erdodi, F., Buday, L., Kardos, J., Kovacs, M., and Nyitray, L. (2010) Affinity, avidity and kinetics of target sequence binding to LC8 dynein light chain isoforms. *J. Biol. Chem. 285*, 38649−38657.

(19) King, S. M., and Patel-King, R. S. (1995) The M(r) = 8,000 and 11,000 outer arm dynein light chains from *Chlamydomonas flagella* have cytoplasmic homologues. *J. Biol. Chem. 270*, 11445−11452.
(20) Espindola, F. S., Suter, D. M., Partata, L. B., Cao, T., Wolenski, J. S., Cheney, R. E., King, S. M., and Mooseker, M. S. (2000) The light chain composition of chicken brain myosin-Va: Calmodulin, myosin-II essential light chains, and 8-kDa dynein light chain/PIN. *Cell Motil. Cytoskeleton 47*, 269−281.
(21) Jaffrey, S. R., and Snyder, S. H. (1996) PIN: An associated protein inhibitor of neuronal nitric oxide synthase. *Science 274*, 774−777.
(22) Chaudhury, A., He, X. D., and Goyal, R. K. (2011) Myosin Va plays a key role in nitrergic neurotransmission by transporting nNOSα to enteric varicosity membrane. *Am. J. Physiol. 301*, G498−G507.
(23) Vadlamudi, R. K., Bagheri-Yarmand, R., Yang, Z., Balasenthil, S., Nguyen, D., Sahin, A. A., den Hollander, P., and Kumar, R. (2004) Dynein light chain 1, a p21-activated kinase 1-interacting substrate, promotes cancerous phenotypes. *Cancer Cell 5*, 575−585.
(24) Lu, J., Sun, Q., Chen, X., Wang, H., Hu, Y., and Gu, J. (2005) Identification of dynein light chain 2 as an interaction partner of p21-activated kinase 1. *Biochem. Biophys. Res. Commun. 331*, 153−158.
(25) Kong, X., Gan, H., Hao, Y., Cheng, C., Jiang, J., Hong, Y., Yang, J., Zhu, H., Chi, Y., Yun, X., and Gu, J. (2009) CDK11p58 phosphorylation of PAK1 Ser174 promotes DLC2 binding and roles on cell cycle progression. *J. Biochem. 146*, 417−427.
(26) Puthalakath, H., Villunger, A., O'Reilly, L. A., Beaumont, J. G., Coultas, L., Cheney, R. E., Huang, D. C., and Strasser, A. (2001) Bmf: A proapoptotic BH3-only protein regulated by interaction with the myosin V actin motor complex, activated by anoikis. *Science 293*, 1829−1832.
(27) Puthalakath, H., Huang, D. C., O'Reilly, L. A., King, S. M., and Strasser, A. (1999) The proapoptotic activity of the Bcl-2 family member Bim is regulated by interaction with the dynein motor complex. *Mol. Cell 3*, 287−296.
(28) Fejtova, A., Davydova, D., Bischof, F., Lazarevic, V., Altrock, W. D., Romorini, S., Schone, C., Zuschratter, W., Kreutz, M. R., Garner, C. C., Ziv, N. E., and Gundelfinger, E. D. (2009) Dynein light chain regulates axonal trafficking and synaptic levels of Bassoon. *J. Cell Biol. 185*, 341−355.
(29) Naisbitt, S., Valtschanoff, J., Allison, D. W., Sala, C., Kim, E., Craig, A. M., Weinberg, R. J., and Sheng, M. (2000) Interaction of the postsynaptic density-95/guanylate kinase domain-associated protein complex with a light chain of myosin-V and dynein. *J. Neurosci. 20*, 4524−4534.
(30) Su, Y., Qiao, W., Guo, T., Tan, J., Li, Z., Chen, Y., Li, X., Li, Y., Zhou, J., and Chen, Q. (2010) Microtubule-dependent retrograde transport of bovine immunodeficiency virus. *Cell. Microbiol. 12*, 1098−1107.
(31) Alonso, C., Miskin, J., Hernaez, B., Fernandez-Zapatero, P., Soto, L., Canto, C., Rodriguez-Crespo, I., Dixon, L., and Escribano, J. M. (2001) African swine fever virus protein p54 interacts with the microtubular motor complex through direct binding to light-chain dynein. *J. Virol. 75*, 9819−9827.
(32) Goddard, T. D., and Kneller, D. G. (2010) *SPARKY 3*, University of California, San Francisco.
(33) Keller, R. (2004) *The Computer Aided Resonance Assignment Tutorial* (Keller, R. L. J., Ed.) Cantina Verlag, Goldau, Switzerland.
(34) Lefevre, J. F., Dayie, K. T., Peng, J. W., and Wagner, G. (1996) Internal mobility in the partially folded DNA binding and dimerization domains of GAL4: NMR analysis of the N-H spectral density functions. *Biochemistry 35*, 2674−2686.
(35) Krizova, H., Zidek, L., Stone, M. J., Novotny, M. V., and Sklenar, V. (2004) Temperature-dependent spectral density analysis applied to monitoring backbone dynamics of major urinary protein-I complexed with the pheromone 2-sec-butyl-4,5-dihydrothiazole. *J. Biomol. NMR 28*, 369−384.
(36) Kabsch, W. (1993) Automatic Processing of Rotation Diffraction Data from Crystals of Initially Unknown Symmetry and Cell Constants. *J. Appl. Crystallogr. 26*, 795−800.
(37) McCoy, A. J., Grosse-Kunstleve, R. W., Storoni, L. C., and Read, R. J. (2005) Likelihood-enhanced fast translation functions. *Acta Crystallogr. D61*, 458−464.
(38) Bailey, S. (1994) The Ccp4 Suite: Programs for Protein Crystallography. *Acta Crystallogr. D50*, 760−763.
(39) Murshudov, G. N., Vagin, A. A., and Dodson, E. J. (1997) Refinement of macromolecular structures by the maximum-likelihood method. *Acta Crystallogr. D53*, 240−255.
(40) Lamzin, V. S., and Wilson, K. S. (1993) Automated refinement of protein models. *Acta Crystallogr. D49*, 129−147.
(41) Emsley, P., and Cowtan, K. (2004) Coot: Model-building tools for molecular graphics. *Acta Crystallogr. D60*, 2126−2132.
(42) Hess, B., Kutzner, C., van der Spoel, D., and Lindahl, E. (2008) GROMACS 4: Algorithms for Highly Efficient, Load-Balanced, and Scalable Molecular Simulation. *J. Chem. Theory Comput. 4*, 435−447.
(43) Ponder, J. W., and Richards, F. M. (1987) An efficient newton-like method for molecular mechanics energy minimization of large molecules. *J. Comput. Chem. 8*, 1016−1024.
(44) Duan, Y., Wu, C., Chowdhury, S., Lee, M. C., Xiong, G., Zhang, W., Yang, R., Cieplak, P., Luo, R., Lee, T., Caldwell, J., Wang, J., and Kollman, P. (2003) A point-charge force field for molecular mechanics simulations of proteins based on condensed-phase quantum mechanical calculations. *J. Comput. Chem. 24*, 1999−2012.
(45) Jorgensen, W. L., Chandrasekhar, J., Madura, J. D., Impey, R. W., and Klein, M. L. (1983) Comparison of simple potential functions for simulating liquid water. *J. Chem. Phys. 79*, 926−935.
(46) Kabsch, W., and Sander, C. (1983) Dictionary of protein secondary structure: Pattern recognition of hydrogen-bonded and geometrical features. *Biopolymers 22*, 2577−2637.
(47) *The PyMOL Molecular Graphics System*, version 1.3r1 (2010) Schrodinger, LLC, Portland, OR.
(48) Lupas, A., Van Dyke, M., and Stock, J. (1991) Predicting coiled coils from protein sequences. *Science 252*, 1162−1164.
(49) Dosztanyi, Z., Csizmok, V., Tompa, P., and Simon, I. (2005) The pairwise energy content estimated from amino acid composition discriminates between folded and intrinsically unstructured proteins. *J. Mol. Biol. 347*, 827−839.
(50) Dosztanyi, Z., Csizmok, V., Tompa, P., and Simon, I. (2005) IUPred: Web server for the prediction of intrinsically unstructured regions of proteins based on estimated energy content. *Bioinformatics 21*, 3433−3434.
(51) Meszaros, B., Simon, I., and Dosztanyi, Z. (2009) Prediction of protein binding regions in disordered proteins. *PLoS Comput. Biol. 5*, e1000376.
(52) Dosztanyi, Z., Meszaros, B., and Simon, I. (2009) ANCHOR: Web server for predicting protein binding regions in disordered proteins. *Bioinformatics 25*, 2745−2746.
(53) Wishart, D. S., Bigam, C. G., Holm, A., Hodges, R. S., and Sykes, B. D. (1995) ^{1}H, ^{13}C and ^{15}N random coil NMR chemical shifts of the common amino acids. I. Investigations of nearest-neighbor effects. *J. Biomol. NMR 5*, 67−81.
(54) Braun, D., Wider, G., and Wuethrich, K. (1994) Sequence-Corrected ^{15}N "Random Coil" Chemical Shifts. *J. Am. Chem. Soc. 116*, 8466−8469.
(55) Mayer, M., and Meyer, B. (2001) Group epitope mapping by saturation transfer difference NMR to identify segments of a ligand in direct contact with a protein receptor. *J. Am. Chem. Soc. 123*, 6108−6117.
(56) Lightcap, C. M., Sun, S., Lear, J. D., Rodeck, U., Polenova, T., and Williams, J. C. (2008) Biochemical and structural characterization of the Pak1-LC8 interaction. *J. Biol. Chem. 283*, 27314−27324.
(57) Benison, G., Karplus, P. A., and Barbar, E. (2007) Structure and dynamics of LC8 complexes with KXTQT-motif peptides: Swallow and dynein intermediate chain compete for a common site. *J. Mol. Biol. 371*, 457−468.
(58) Williams, J. C., Roulhac, P. L., Roy, A. G., Vallee, R. B., Fitzgerald, M. C., and Hendrickson, W. A. (2007) Structural and thermodynamic characterization of a cytoplasmic dynein light chain-

intermediate chain complex. *Proc. Natl. Acad. Sci. U.S.A. 104*, 10028−10033.
(59) Hall, J., Karplus, P. A., and Barbar, E. (2009) Multivalency in the assembly of intrinsically disordered Dynein intermediate chain. *J. Biol. Chem. 284*, 33115−33121.
(60) Kiss, R., Kovacs, D., Tompa, P., and Perczel, A. (2008) Local structural preferences of calpastatin, the intrinsically unstructured protein inhibitor of calpain. *Biochemistry 47*, 6936−6945.
(61) Szalaine Agoston, B., Kovacs, D., Tompa, P., and Perczel, A. (2011) Full backbone assignment and dynamics of the intrinsically disordered dehydrin ERD14. *Biomol. NMR Assignments 5*, 189−193.
(62) Csizmok, V., Felli, I. C., Tompa, P., Banci, L., and Bertini, I. (2008) Structural and dynamic characterization of intrinsically disordered human securin by NMR spectroscopy. *J. Am. Chem. Soc. 130*, 16873−16879.
(63) Oldfield, C. J., Meng, J., Yang, J. Y., Yang, M. Q., Uversky, V. N., and Dunker, A. K. (2008) Flexible nets: Disorder and induced fit in the associations of p53 and 14-3-3 with their partners. *BMC Genomics 9* (Suppl. 1), S1.
(64) Benison, G., Nyarko, A., and Barbar, E. (2006) Heteronuclear NMR identifies a nascent helix in intrinsically disordered dynein intermediate chain: Implications for folding and dimerization. *J. Mol. Biol. 362*, 1082−1093.
(65) Benison, G., and Barbar, E. (2009) NMR analysis of dynein light chain dimerization and interactions with diverse ligands. *Methods Enzymol. 455*, 237−258.
(66) Stein, A., and Aloy, P. (2008) Contextual specificity in peptide-mediated protein interactions. *PLoS One 3*, e2524.
(67) Sellers, J. R., Thirumurugan, K., Sakamoto, T., Hammer, J. A., III, and Knight, P. J. (2008) Calcium and cargoes as regulators of myosin 5a activity. *Biochem. Biophys. Res. Commun. 369*, 176−181.
(68) Li, X. D., Jung, H. S., Mabuchi, K., Craig, R., and Ikebe, M. (2006) The globular tail domain of myosin Va functions as an inhibitor of the myosin Va motor. *J. Biol. Chem. 281*, 21789−21798.
(69) Thirumurugan, K., Sakamoto, T., Hammer, J. A., III, Sellers, J. R., and Knight, P. J. (2006) The cargo-binding domain regulates structure and activity of myosin 5. *Nature 442*, 212−215.
(70) Krementsov, D. N., Krementsova, E. B., and Trybus, K. M. (2004) Myosin V: Regulation by calcium, calmodulin, and the tail domain. *J. Cell Biol. 164*, 877−886.
(71) Nyarko, A., Hare, M., Hays, T. S., and Barbar, E. (2004) The intermediate chain of cytoplasmic dynein is partially disordered and gains structure upon binding to light-chain LC8. *Biochemistry 43*, 15595−15603.
(72) Wang, L., Hare, M., Hays, T. S., and Barbar, E. (2004) Dynein light chain LC8 promotes assembly of the coiled-coil domain of swallow protein. *Biochemistry 43*, 4611−4620.
(73) Hornbeck, P. V., Kornhauser, J. M., Tkachev, S., Zhang, B., Skrzypek, E., Murray, B., Latham, V., and Sullivan, M. (2012) PhosphoSitePlus: A comprehensive resource for investigating the structure and function of experimentally determined post-translational modifications in man and mouse. *Nucleic Acids Res. 40*, D261−D270.
(74) Komander, D. (2009) The emerging complexity of protein ubiquitination. *Biochem. Soc. Trans. 37*, 937−953.
(75) Fuxreiter, M., Tompa, P., and Simon, I. (2007) Local structural disorder imparts plasticity on linear motifs. *Bioinformatics 23*, 950−956.
(76) Dou, Y., Baisnee, P. F., Pollastri, G., Pecout, Y., Nowick, J., and Baldi, P. (2004) ICBS: A database of interactions between protein chains mediated by β-sheet formation. *Bioinformatics 20*, 2767−2777.
(77) Hoskins, J., Lovell, S., and Blundell, T. L. (2006) An algorithm for predicting protein-protein interaction sites: Abnormally exposed amino acid residues and secondary structure elements. *Protein Sci. 15*, 1017−1029.